Fig. 6

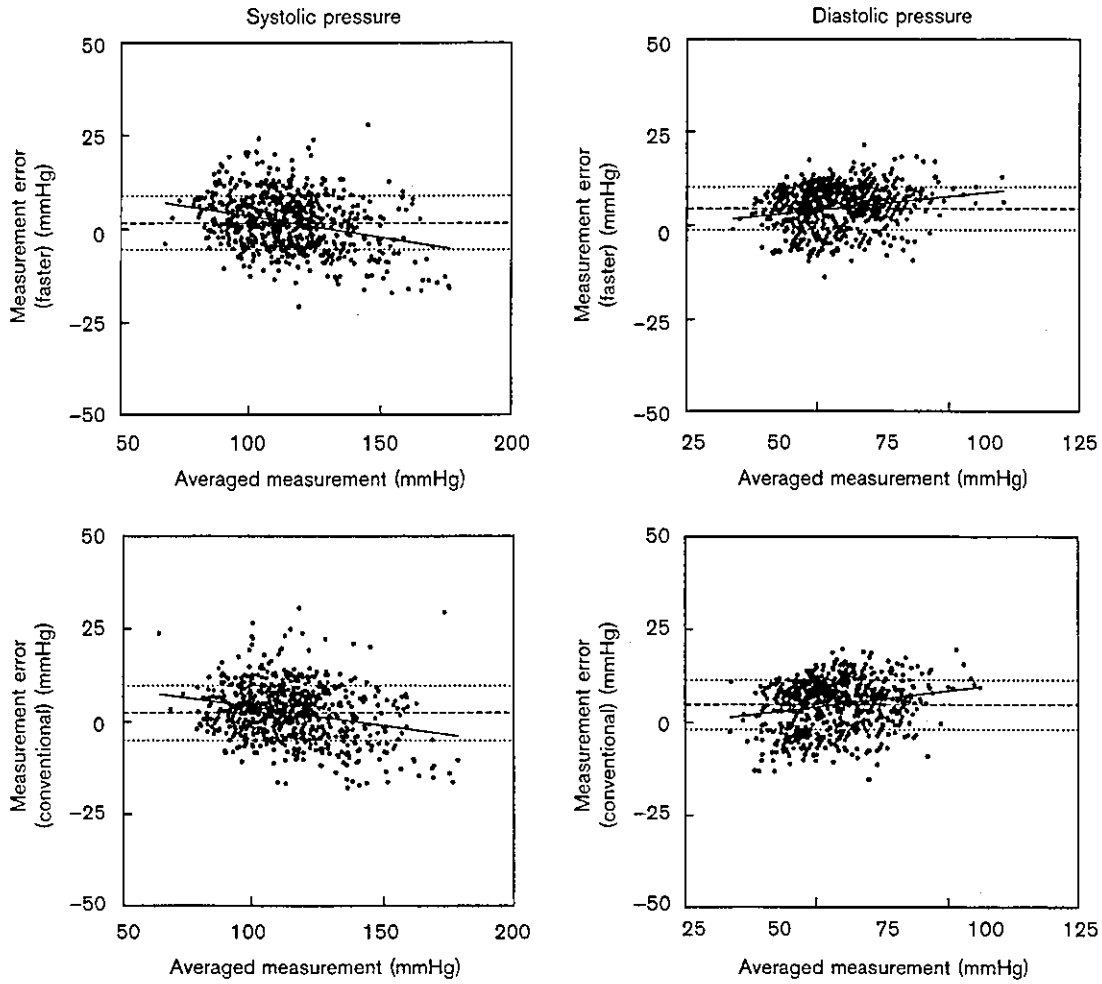

Bland-Altman plots examining the measurement errors (oscillometric minus invasive pressure) of systolic (left) and diastolic (right) pressure and their dependence on pressure values (average of oscillometric and invasive pressure). Plots are shown for the conventional (bottom) and the faster (top) oscillometry. Solid lines indicate the regression line, dashed lines indicate the mean error, and dotted lines the mean ± SD of the error.

decreases the number of heartbeats available for pressure determination. Without interpolation or curve fitting, oscillometric accuracy would have drastically worsened.

On the other hand, we consider that the linearization of the cuff deflation somewhat contributed to the accuracy. In fact, the mean error for the systolic pressure and the SD error for the diastolic pressure are smaller using the faster oscillometric technique.

Besides the fact that faster oscillometry can track rapid pressure changes it is favourable from the viewpoint of patients' comfort. Some patients might complain of pains in the upper extremities with sustained arm compression by cuff; the accelerated deflation would be favourable in these patients. Our oscillometry did not increase cuff inflation speed because this is likely to increase pain.

In conclusion, by acceleration and linearization of cuff deflation and by interpolation of the relationship between cuff pressure and oscillometric wave amplitude, we succeeded in shortening the pressure measurement time to approximately 60% of the original without sacrificing measurement accuracy.

Acknowledgements

This study was supported by the Program for Promotion of Fundamental Studies in Health Science of the Organization for Pharmaceutical Safety and Research of Japan, and a Health and Labour Sciences Research Grant (Research on Advanced Medical Technology, H14-nano-002) from the Ministry of Health, Labour and Welfare of Japan.

Fig. 7

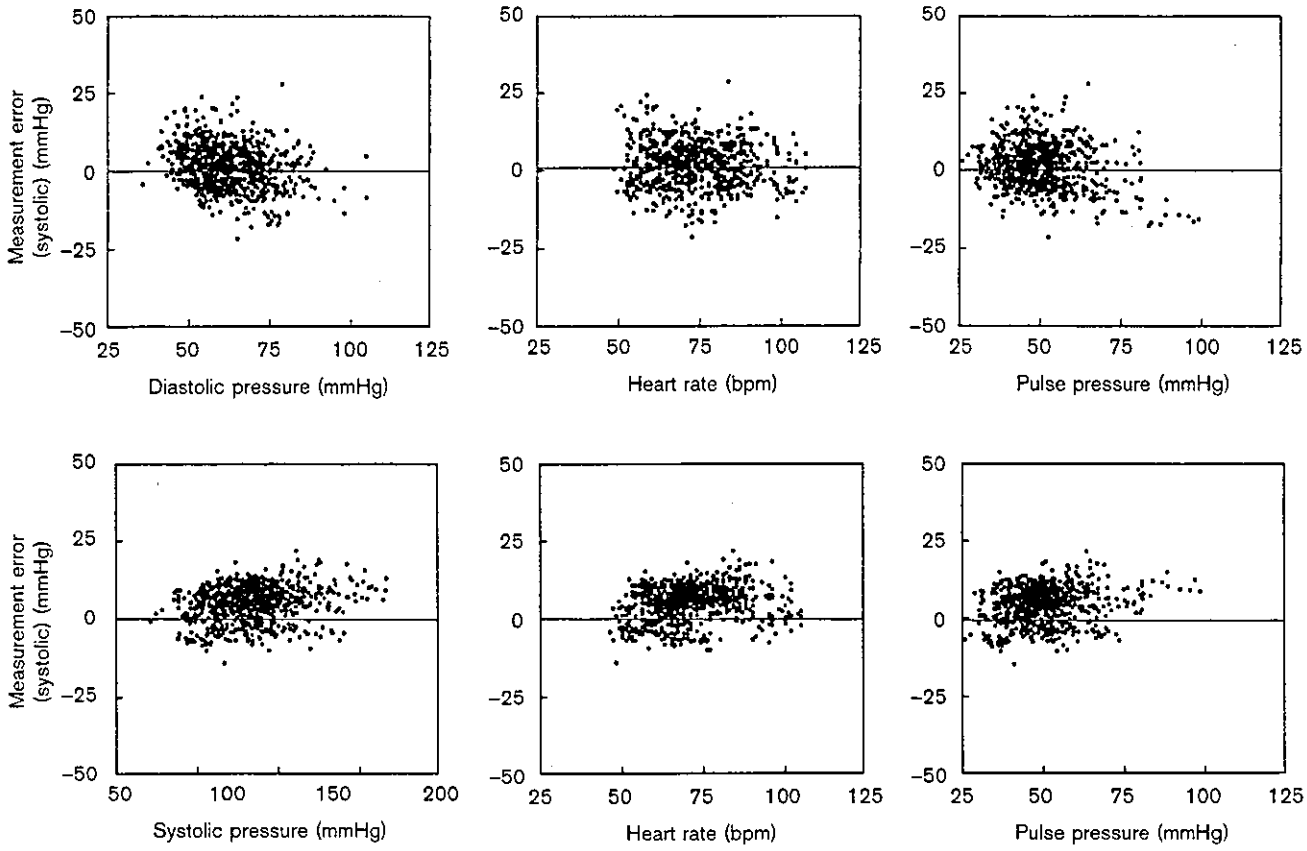

Scatterplots examining the dependence of the measurement errors for systolic (top) and diastolic (bottom) pressure using the faster oscillometry on other pressure values and heart rate. The average oscillometric and invasive pressure values were used for the independent variables.

References

1 Bland JM, Altman DG. Statistical methods for assessing agreement between two methods of clinical measurement. *Lancet* 1986; 1:307–310.

2 Bland JM, Altman DG. Comparing methods of measurement: why plotting difference against standard method is misleading. *Lancet* 1995; **346**: 1085–1087.

3 O'Rourke MF, Kelly R, Avolio A. *The Arterial Pulse*. Philadelphia, PA. Lea & Febiger; 1992.

4 Bur A, Herkner H, Vlcek M, Woisetschlager C, Derhaschnig U, Delle Karth G, *et al.* Factors influencing the accuracy of oscillometric blood pressure measurement in critically ill patients. *Crit Care Med* 2003; **31**:793–797.

5 O'Brien E, Petrie J, Litter W, de Swiet M, Padfield OL, Altman DG, *et al.* The British Hypertension Society protocol for the evaluation of blood pressure measuring devices. *J Hypertens* 1993; **11(Suppl 2)**:S43–S62.

6 ANSI/AAMI SP10: 2002. *Manual, Electronic or Automated Sphygnomanometers*. Arlington, VA. Association for the Advancement of Medical Instrumentation. 2003.

7 Ling J, Ohara Y, Orime Y, Noon GP, Takatani S. Clinical evaluation of the oscillometric blood pressure monitor in adults and children based on the 1992 AAMI SP-10 standards. *J Clin Monit* 1995; **11**:123–130.

8 Hersh LT, Friedman B, Medero R. Method for oscillometric blood pressure determination employing curve fitting. United States Patent 5704362, January 6, 1998, assigned to Johnson & Johnson Medical, Inc.

9 Friedman B, Hersh LT, Medero R. Calculation of quality and its use in determination of indirect non-invasive blood pressure. United States Patent 6358213, Mar 19, 2002, assigned to Critikon Company, LLC.

J Appl Physiol 97: 984–990, 2004.
First published May 7, 2004; 10.1152/japplphysiol.00162.2004.

Bionic epidural stimulation restores arterial pressure regulation during orthostasis

Yusuke Yanagiya,[1,2] Takayuki Sato,[1,3] Toru Kawada,[1] Masashi Inagaki,[1] Teiji Tatewaki,[1,4] Can Zheng,[1,2] Atsunori Kamiya,[1] Hiroshi Takaki,[1] Masaru Sugimachi,[1] and Kenji Sunagawa[1]

[1]*Department of Cardiovascular Dynamics, National Cardiovascular Center Research Institute, Suita, Osaka 565-8565;*
[2]*Pharmaceuticals and Medical Devices Agency, Chiyoda-ku, Tokyo 100-0013;*
[3]*Department of Cardiovascular Control, Kochi Medical School, Nankoku, Kochi 783-8505;*
and [4]*Japan Association for the Advancement of Medical Equipment, Bunkyo-ku, Tokyo 113-0033, Japan*

Submitted 13 February 2004; accepted in final form 30 April 2004

Yanagiya, Yusuke, Takayuki Sato, Toru Kawada, Masashi Inagaki, Teiji Tatewaki, Can Zheng, Atsunori Kamiya, Hiroshi Takaki, Masaru Sugimachi, and Kenji Sunagawa. Bionic epidural stimulation restores arterial pressure regulation during orthostasis. *J Appl Physiol* 97: 984–990, 2004. First published May 7, 2004; 10.1152/japplphysiol.00162.2004.—A bionic baroreflex system (BBS) is a computer-assisted intelligent feedback system to control arterial pressure (AP) for the treatment of baroreflex failure. To apply this system clinically, an appropriate efferent neural (sympathetic vasomotor) interface has to be explored. We examined whether the spinal cord is a candidate site for such interface. In six anesthetized and baroreflex-deafferentiated cats, a multielectrode catheter was inserted into the epidural space to deliver epidural spinal cord stimulation (ESCS). Stepwise changes in ESCS rate revealed a linear correlation between ESCS rate and AP for ESCS rates of 2 pulses/s and above (r^2, 0.876–0.979; slope, 14.3 ± 5.8 mmHg·pulses^{-1}·s; pressure axis intercept, 35.7 ± 25.9 mmHg). Random changes in ESCS rate with a white noise sequence revealed dynamic transfer function of peripheral effectors. The transfer function resembled a second-order, low-pass filter with a lag time (gain, 16.7 ± 8.3 mmHg·pulses^{-1}·s; natural frequency, 0.022 ± 0.007 Hz; damping coefficient, 2.40 ± 1.07; lag time, 1.06 ± 0.41 s). On the basis of the transfer function, we designed an artificial vasomotor center to attenuate hypotension. We evaluated the performance of the BBS against hypotension induced by 60° head-up tilt. In the cats with baroreflex failure, head-up tilt dropped AP by 37 ± 5 mmHg in 5 s and 59 ± 11 mmHg in 30 s. BBS with optimized feedback parameters attenuated hypotension to 21 ± 2 mmHg in 5 s ($P < 0.05$) and 8 ± 4 mmHg in 30 s ($P < 0.05$). These results indicate that ESCS-mediated BBS prevents orthostatic hypotension. Because epidural stimulation is a clinically feasible procedure, this BBS can be applied clinically to combat hypotension associated with various pathophysiologies.

baroreceptors; blood pressure; autonomic nervous system; Shy-Drager syndrome; orthostatic hypotension

THE ARTERIAL BAROREFLEX SYSTEM configures a negative feedback system and reduces arterial pressure (AP) disturbances from external influences (9, 15, 22, 23). Sudden onset of hypotension by orthostatic change occurs as a result of baroreflex failure, despite normal functioning of the cardiovascular system and efferent sympathetic nervous system. This condition is seen in multiple-system atrophy (Shy-Drager syndrome) (21, 22, 30) as well as spinal cord injuries (7, 17). Current treatments, such as salt loading (19, 33), cardiac pacing (1, 14), and pharmacological interventions (2, 3, 12, 20), fail to prevent the orthostatic hypotension. These therapies often result in an unwanted increase in AP in the supine position and neither restore nor reproduce the function of the feedback system that forms the basis of AP control (See DISCUSSION).

Previously, our laboratory developed a bionic baroreflex system (BBS) that substitutes the defective vasomotor center with an artificial controller (i.e., an artificial vasomotor center) to restore the native baroreflex function (24, 26). In these animal studies, the celiac ganglion was exposed by laparotomy and stimulated directly as the efferent neural interface in the BBS. However, for clinical application of the BBS, a less invasive and more stable electrical stimulation method is required.

In the present study, we examined the hypothesis that the spinal cord is a candidate site for the efferent neural interface in our bionic strategy. Epidural spinal cord stimulation (ESCS) has been used for the management of patients with malignant neoplasm, angina pectoris, and peripheral ischemia (6, 29). Stimulating the dorsal part of the spinal cord changes sympathetic nerve activity, AP in animals (11, 32) and heart rate in humans (18). If we can delineate how ESCS affects AP quantitatively, then this may lead to clinical application of the BBS. We studied the feasibility of ESCS-mediated BBS using an animal model of central baroreflex failure.

MATERIALS AND METHODS

Study design. BBS is a negative feedback system and consists of two components: peripheral effectors and the artificial vasomotor center (Fig. 1). Peripheral effectors change AP in response to ESCS. The artificial vasomotor center (controller) determines the ESCS rate in response to changes in AP. Using BBS, we computer programmed the artificial vasomotor center and substituted the defective vasomotor center with an artificial vasomotor center.

For this purpose, we first characterized the static as well as dynamic responses of the peripheral effectors. With this knowledge, we then designed an artificial vasomotor center using simulation to delineate the parameters for obtaining optimal AP response. Finally, we evaluated the performance of the ESCS-mediated BBS in cats during orthostatic AP changes.

Animals and surgical procedures. Animals were cared for in strict accordance with the "Guiding Principles for the Care and Use of Animals in the Field of Physiological Sciences," approved by the Physiological Society of Japan. Six adult cats of either sex, weighing

Address for reprint requests and other correspondence: M. Sugimachi, Dept. of Cardiovascular Dynamics, National Cardiovascular Center Research Institute, 5-7-1 Fujishirodai, Suita 565–8565, Japan.

The costs of publication of this article were defrayed in part by the payment of page charges. The article must therefore be hereby marked "*advertisement*" in accordance with 18 U.S.C. Section 1734 solely to indicate this fact.

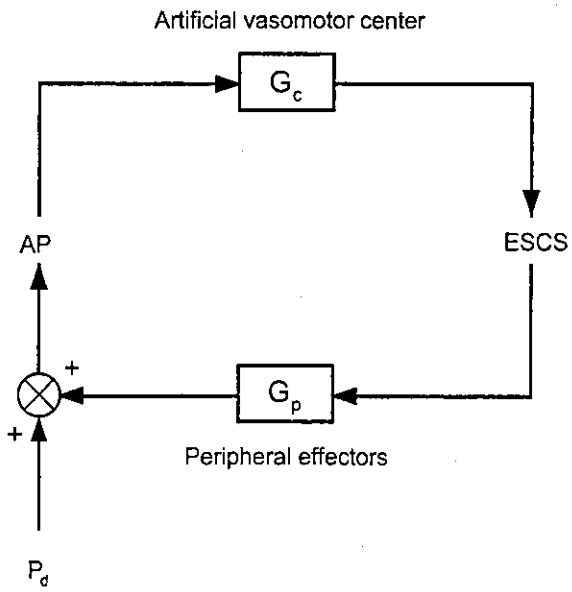

Fig. 1. Simplified diagram of bionic baroreflex system (BBS) using epidural spinal cord stimulation (ESCS). Peripheral effectors change arterial pressure (AP) in response to ESCS. The artificial vasomotor center determines ESCS rate in response to changes in AP. Transfer function of the peripheral effectors (G_p) cannot be controlled, but the vasomotor center transfer function (G_c) can be computer programmed as needed. P_d, pressure disturbance to AP.

1.6–3.7 kg, were premedicated with ketamine (5 mg/kg im) and then anesthetized by intraperitoneal injection (1.0 ml/kg) of a mixture of urethane (250 mg/ml) and α-chloralose (40 mg/ml).

For AP measurement, a high-fidelity pressure transducer (SPC-320, Millar Instruments, Houston, TX) was placed in the aortic arch via the right femoral artery. Pancronium bromide (0.3 mg/kg) was administered to prevent muscular activity. The cats were mechanically ventilated with oxygen-enriched room air. Body temperature was maintained at around 38°C with a heating pad. To produce the baroreflex failure model, the carotid sinus, aortic depressor, and vagal nerves were sectioned bilaterally. The rationale for using baroreceptor-deafferentiated animals as the baroreflex failure model is that, in patients with multiple-system atrophy, the reason for sudden hypotension induced by orthostatic change is a lack of reflex control of AP sensed at the baroreceptors.

A partial laminectomy was performed in the L_3 vertebra to expose the dura mater. A multielectrode catheter with interelectrode distance of 10 mm was introduced rostrally ~7 cm into the epidural space. The stimulating electrodes were positioned on the dorsal surface of the spinal cord within T_{12}, T_{13}, and L_1. These spinal levels were selected because our preliminary studies showed that ESCS to these levels produced greater AP response compared with other spinal levels. The catheter was connected to an isolated electric stimulator (SS-102J and SEN7203, Nihon Kohden, Tokyo, Japan) via a custom-made, constant-voltage amplifier. The stimulator was controlled with a laboratory computer (PC9801FA, NEC, Tokyo, Japan).

Data recording for characterizing AP response to ESCS. To characterize the static as well as dynamic AP responses to ESCS, we measured AP responses while changing ESCS rate. To estimate static response, we changed the ESCS rate sequentially in stepwise increments and decrements. Each stimulation step was maintained for 90 s. To estimate dynamic response, we randomly changed the ESCS rate, according to a binary white noise sequence with a minimum sequence length of 1 s. In both protocols, the stimulation voltage was fixed at 5 V, and the pulse width of the stimulus was 1 ms. While the stimulation was given, ESCS rate and AP were digitized at a rate of 200 Hz with a 12-bit resolution analog-to-digital converter [AD12–8 (PM), Contec, Osaka, Japan] and stored in another laboratory computer (PC98-NX VA70J, NEC). In this study, "ESCS rate" is defined as the number of stimulation pulses per second and is distinguished from the term "frequency," which refers to how frequently ESCS rate changes.

Estimation of static AP response parameters. We parameterized the static AP response to ESCS. Each steady-state AP value was obtained by averaging the AP during the last 10 s of each ESCS step. Stimulation at low-ESCS rate decreased AP, but stimulation at higher rates increased AP. We fit both responses together to a linear regression model of AP vs. ESCS rate. We determined the rate at which the pressor and depressor effects balanced and designated it the offset stimulation rate (s_o).

Estimation of peripheral effector transfer function. The transfer function of the peripheral effector was estimated by using a white noise method described in detail elsewhere (10, 13, 16, 24–26, 31). Briefly, on the basis of the resampled data at 10 Hz, the linear transfer function from ESCS rate to AP was calculated as a quotient of the ensemble average of cross-power between the two and that of ESCS rate power. The transfer function was calculated up to 0.5 Hz with a resolution of 0.0098 Hz. We parameterized the transfer function by using an iterative, nonlinear, least squares fitting technique (10).

Design of central characteristics and implementation by the artificial vasomotor center. Based on the parameterized effector transfer function, we designed the vasomotor center transfer function using computer simulation. The characteristics of the vasomotor center have been identified as derivative characteristics in rabbits and rats (10, 13, 25). We did not have the corresponding data for cats but assumed that they resembled those in rabbits and rats. We adjusted the parameters by simulation, aiming to attenuate hypotension to ~20 mmHg within 5 s and to ≤10 mmHg at 30 s. We implemented designed transfer function by the artificial vasomotor center with convolution algorithm (see APPENDIX).

Head-up tilt tests. The efficacy of the BBS against orthostatic stress was evaluated in each animal by the head-up tilt (HUT) test. We placed baroreflex failure animals in a prone position on a custom-made tilt table and measured AP responses to 60° HUT, with or without BBS activation. In the absence of BBS control, we fixed the ESCS rate at s_o, irrespective of AP changes. The BBS was activated by sending ESCS command to the stimulator, as calculated by the artificial vasomotor center in response to AP change. Tilt angle, ESCS rate, and AP were stored in a laboratory computer.

Statistical analysis. All data are presented as means ± SD. We analyzed AP responses at 5 and 30 s after HUT. AP changes from control value were compared among protocols by using repeated-measures analysis of variance followed by Dunnett's multiple-comparison procedure (8). Differences were considered significant when $P < 0.05$.

RESULTS

Figure 2*A* is a representative example of static AP response to stepwise ESCS changes. Stepwise increases of ESCS rate produced a depressor response initially at low-ESCS rate and a pressor response at higher rates, and subsequent decreases of ESCS rate produced almost perfect reversal of AP changes. The relationship between AP and ESCS rate appeared nonlinear as a whole (Fig. 2*B*, *top*). However, for ESCS rates of 2 pulses/s and above, there is a linear relationship ($r^2 = 0.964$, AP = 16.0 × ESCS + 44.0, s_o = 3.2 pulses/s; Fig. 2*B*). A linear relationship during ESCS was found in all animals [r^2, 0.876–0.979 (median, 0.959) slope, 14.3 ± 5.8 mmHg·pulses^{-1}·s; pressure axis intercept, 35.7 ± 25.6 mmHg; s_o, 4.9 ± 2.5 pulses/s]. The following protocols were performed by using this linear ESCS range.

Figure 3*A* is a representative example of dynamic AP response to ESCS. We selected low- and high-stimulation rates that produced depressor and pressor responses, respectively,

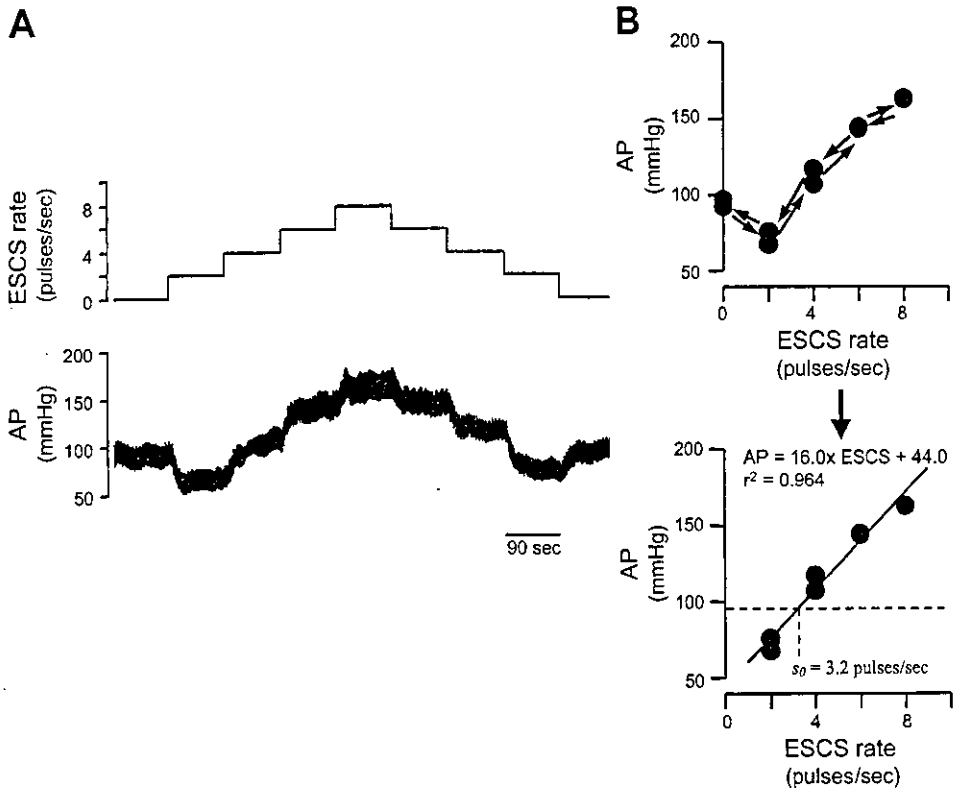

Fig. 2. *A*: representative time series of static AP response to ESCS. Stepwise increases of ESCS rate produced a depressor response initially at low-ESCS rate and a pressor response at higher rates, and subsequent decreases of ESCS rate produced almost perfect reversal of AP changes. *B*: procedures to estimate steady-state relationship between AP and ESCS rate. Each steady-state AP value was plotted against ESCS rate (*top*). Although the relationship between AP and ESCS rate appears nonlinear as a whole, linear regression analysis was conducted for the data obtained during ESCS (2, 4, 6, and 8 Hz), omitting the values before and after ESCS (0 Hz). A linear relationship is obtained. The value s_0 represents the stimulation rate where pressor and depressor responses balance.

and stimulated the spinal cord, according to a binary white noise sequence. AP did not respond to fast changes in ESCS rate, but appeared to respond to slower changes, increasing with high-rate stimulation and decreasing with low-rate stimulation. The estimated transfer function indicated low-pass filter characteristics. Figure 3*B* shows the averaged transfer function from ESCS rate to AP in six animals. The gain decreased as the frequency increased and was attenuated to one-tenth of the lowest frequency at 0.1 Hz. The phase approached zero radian at the lowest frequency, reflecting in-phase changes of ESCS rate and AP. The parameters obtained by the least squares fitting to the second-order, low-pass filter model are as follows: dynamic gain = 16.7 ± 8.3 mmHg·pulses^{-1}·s, natural frequency = 0.022 ± 0.007 Hz, damping coefficient = 2.40 ± 1.07, and lag time = 1.06 ± 0.41 s. The dynamic gain was much higher than the gain at the lowest frequency in the transfer function (Fig. 3A) but comparable to the slope obtained in the static protocol. The coherence function was close to unity between 0.01 and 0.4 Hz, indicating that the input-output relation was governed by almost linear

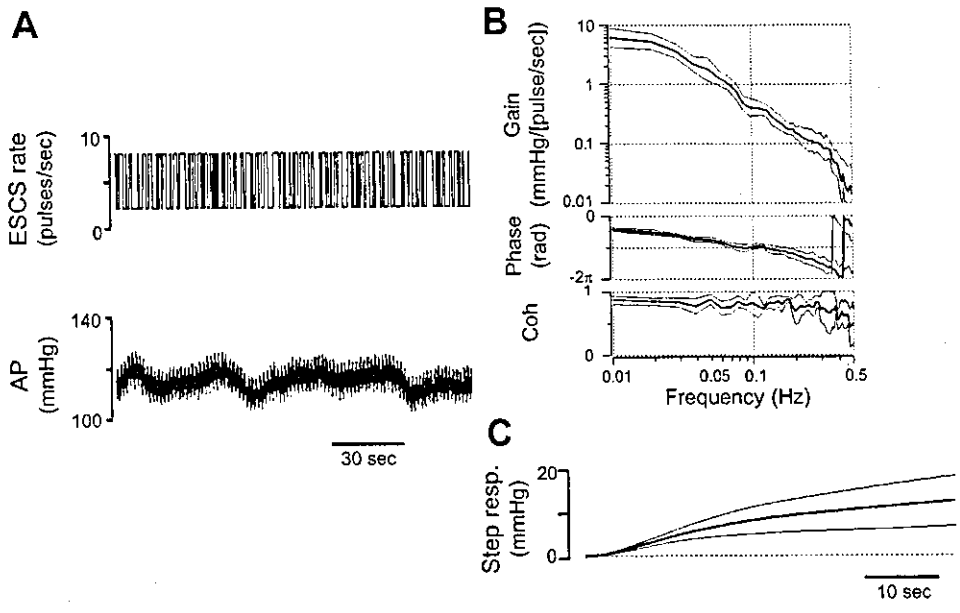

Fig. 3. *A*: representative example of dynamic AP response to ESCS. *B*: averaged transfer functions from ESCS rate to AP, i.e., G_p (gain and phase) and coherence function (Coh). *C*: estimated step response (resp) computed from the transfer function. Data are expressed as means ± SD for 6 cats.

dynamics in this range. To facilitate better understanding of the dynamic AP response to ESCS, the step functions were calculated by time integral of the inverse Fourier transform of the transfer functions. The estimated step functions are averaged and shown in Fig. 3*C*. An initial time lag and overdamped slow AP response to unit step ESCS are evident. The time courses of the estimated step functions were almost identical to but smoother than those of the actually observed AP responses to stepwise ESCS changes, indicating the ability to cancel out noises by the white noise method.

Figure 4 is a representative example of how we designed the vasomotor center transfer function. The steady-state gain is determined simply to match a total baroreflex loop gain of 5. This setting ensures that the steady-state AP fall will be attenuated to 10 mmHg in the case of a depressor stimulus of 60 mmHg. By changing the derivative corner frequency (f_c), we simulated various transient AP responses to orthostatic depressor stimulation. Lower f_c causes unstable oscillation in AP (Fig. 4*B*, *left*), and higher f_c slows AP restoration (Fig. 4*B*, *right*). On the basis of these simulations, f_c = 0.02 Hz was selected in this example (Fig. 4*B*, *middle*, 0.018 ± 0.008 Hz in 6 cats).

Figure 5 shows a representative example of real-time application of BBS to a cat. In the control cat with baroreflex failure, abrupt HUT produced a rapid and then progressive fall in AP by 44 mmHg in 30 s (Fig. 5, *left*). Activation of the simulation-based BBS attenuated the AP fall (Fig. 5, *middle*; AP fall, 25 mmHg in 5 s and 19 mmHg in 30 s) but did not attain the predetermined target (gaps indicated by vertical bars in Fig. 5, *middle* and *right*). If the total loop gain of 5 were preserved, the AP fall should theoretically be attenuated to 44/(1 + 5), or ~7 mmHg, according to the linear control theory. The observed attenuation of 19/44 (=1/2.3) indicated that the actual gain was 1.3 (1 + 1.3 = 2.3). To achieve a total loop gain of 5, we increased the gain of the vasomotor center transfer function by 3.8-fold and reassessed the efficacy of BBS. As a result, AP returned to the predetermined target (Fig. 5, *right*; AP fall, 19 mmHg in 5 s, 7 mmHg in 30 s).

Figure 6 summarizes the results obtained from six cats, demonstrating the effectiveness of the BBS performance. In the cat model of baroreflex failure, HUT decreased AP by 37 ± 5 mmHg in 5 s and by 59 ± 11 mmHg in 30 s. In animals with simulation-based vasomotor center, the initial attenuation (AP fall: 32 ± 7 mmHg in 5 s) was not significant, and the steady-state attenuation (17 ± 8 mmHg in 30 s) did not satisfy the predetermined target. On the other hand, in animals with gain-adjusted vasomotor center (2.4 ± 1.1-fold increase), the BBS achieved both initial and the steady-state targets (21 ± 2 mmHg in 5 s, $P < 0.05$; 8 ± 4 mmHg in 30 s, $P < 0.05$).

DISCUSSION

The present results indicate that AP can be controlled by ESCS and that ESCS-mediated BBS prevents orthostatic hypotension in anesthetized cats. Although the BBS based on simulation alone did not work as predicted during HUT, gain adjustments of the vasomotor center achieved quick and stable restoration of AP.

Necessity of BBS for treatment of central baroreflex failure. Conventional treatments for central baroreflex failure aim at increasing AP. Although they alleviate the hypotension to the extent of preventing syncope, they have adverse effects of causing supine hypertension and enhancing the risk of hypertensive organ disease. Recently, Shannon et al. (28) suggested well-timed water consumption as a treatment for orthostatic hypotension in patients with autonomic failure. Their strategy is superior to conventional treatments because it prevents AP fall if predicted in advance. However, at least a few minutes are necessary for their method to increase AP. This time lag makes it impossible to control AP against sudden or unpredictable AP

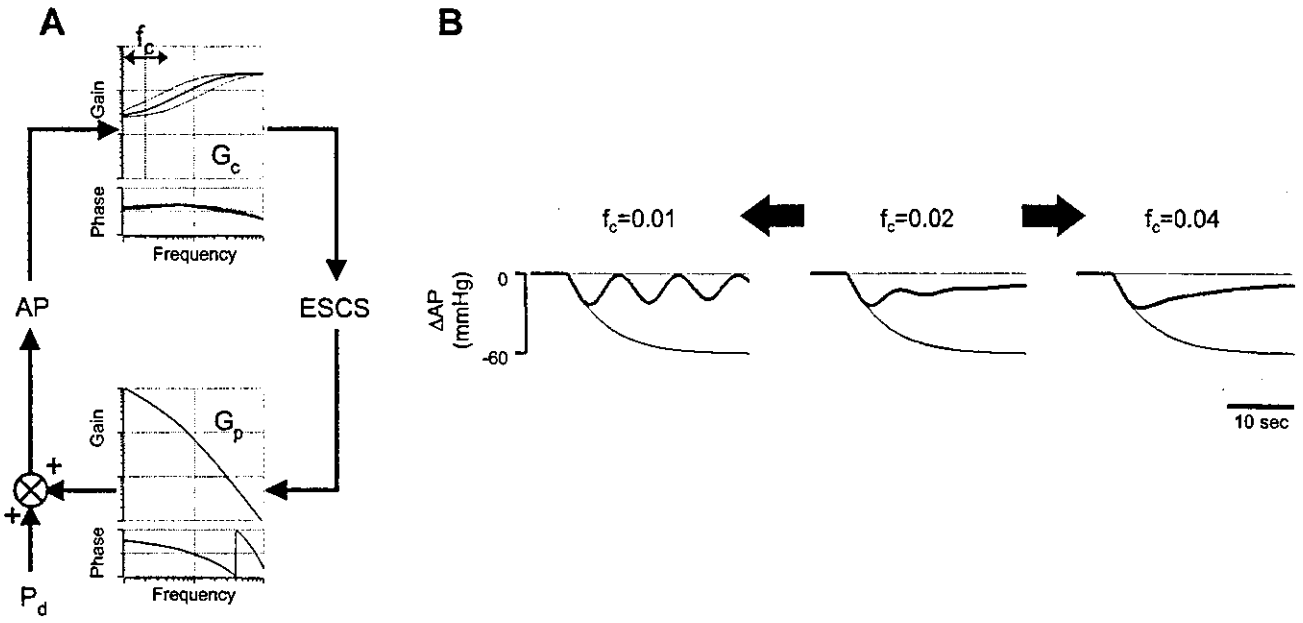

Fig. 4. Representative example of designing the G_c. *A*: schematic diagram of the method of designing the G_c. AP changes in the presence of P_d were simulated by changing the corner frequency (f_c) for derivative characteristic in the G_c. *B*: simulation results of this example. A vasomotor center with f_c of 0.02 Hz restores AP with sufficient speed and stability (center).

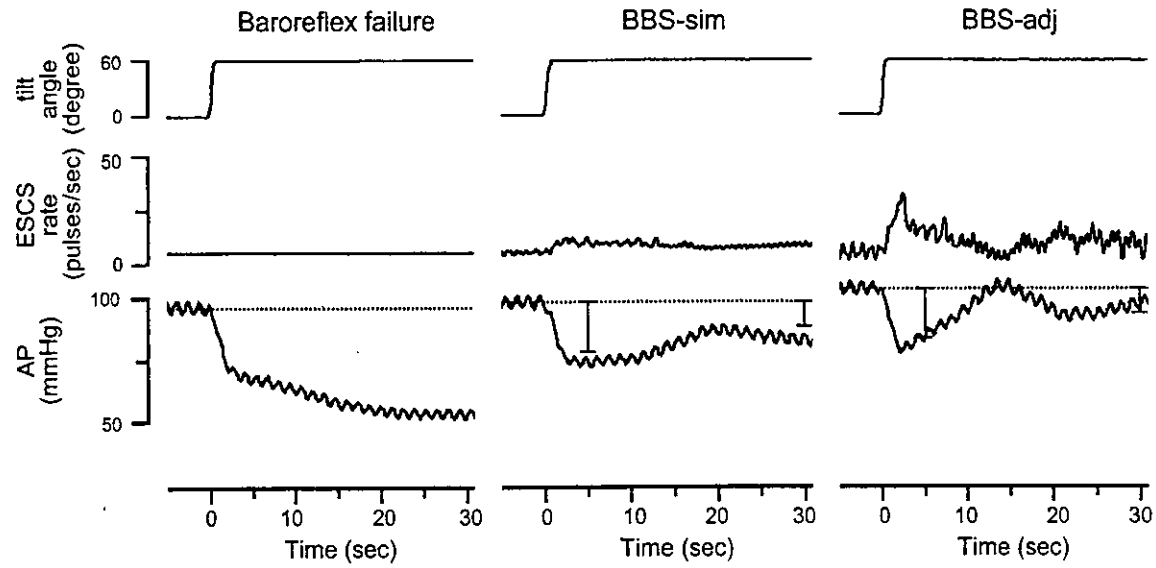

Fig. 5. Representative example of real-time application of the BBS during head-up tilt (HUT). *Left*: in the cat with baroreflex failure, ESCS rate was fixed at 5.0 pulse/s. HUT produced a rapid and then progressive fall in AP. *Middle*: simulation-based BBS (BBS-sim) attenuated the AP fall but did not attain the predetermined target. *Right*: gain adjustment of the vasomotor center (BBS-adj) resulted in quick and sufficient attenuation of AP fall (see text for detail). Vertical bars indicate the ranges of predetermined targets.

fall. None of the treatments attempted so far can prevent sudden orthostatic hypotension because the dynamics of the baroreflex remain impaired.

In contrast, the BBS continuously monitors and controls AP to achieve quick restoration of AP. Because AP is increased via sympathetic pathways, the AP response to the BBS vasomotor center command is as fast as that to the native vasomotor center control. Therefore, the quick, adequate, and stable nature of the native baroreflex system can be restored by the BBS with appropriate settings of the artificial vasomotor center.

Designing the vasomotor center transfer function and parameter adjustments. In a negative feedback system, closed-loop responses to external perturbation are dependent on the dynamic characteristics of the total open-loop transfer function. We assumed that the derivative characteristics in cats are identical to those in rabbits or rats, which have been delineated previously (10, 13, 25). We optimized gain and derivative parameters for each cat so that both speed and stability were achieved.

In animal experiments, however, the simulation results were not fully reproduced. Gain adjustments of the vasomotor center were necessary to attain quick and sufficient attenuation of the AP fall. This discrepancy cannot be explained without considering a possible slope decrease or nonlinearity in peripheral effector characteristics (AP-ESCS relationship) caused by the HUT, or both. Pooling of blood volume in the splanchnic and hindlimb circulation would be a cause for such attenuated AP response. If AP responses during posture change can be de-

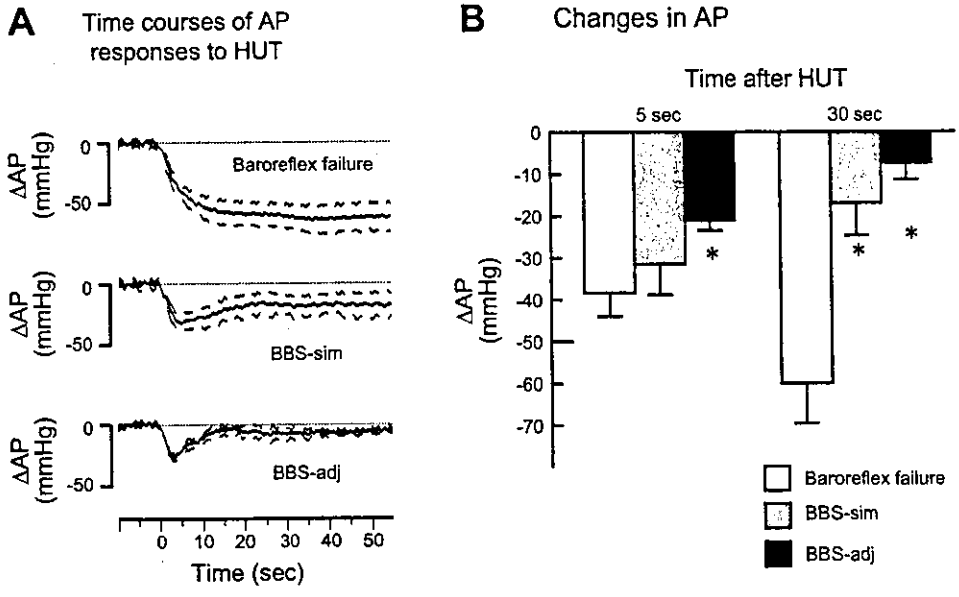

Fig. 6. Summarized results of HUT obtained from 6 cats. *A*: averaged time courses of AP responses to HUT in cats with baroreflex failure (*top*) and with BBS (*middle* and *bottom*). Using the parameters determined from simulation, we found that the BBS (BBS-sim) did not adequately attenuate hypotension in all cats (*middle*). Appropriate gain increase (BBS-adj) was necessary for quick and sufficient attenuation of hypotension (*bottom*). *B*: changes in AP produced by HUT. Data are expressed as means ± SD. $^*P < 0.05$ compared with baroreflex failure.

fined quantitatively, then a more elaborate artificial vasomotor center can be developed that automatically adjusts the parameters. Automated adjustments may also be accomplished with adaptive control systems that execute real-time system identification and self-tuning of controller. The present study suggests the necessity of such manipulation of the vasomotor center settings.

Pressor and depressor responses by ESCS. We demonstrated both depressor and pressor responses in AP to ESCS with a linear range (Fig. 2). Earlier studies have shown that dorsal column stimulation produces pressor and depressor responses. Depressor response is produced by a group of dorsal column fibers that project to the dorsal nuclei at the level of C_8 to L_1 and transmit to the fibers that ascend through the dorsal spinocerebeller tracts (4, 27, 32). Pressor response is produced by another group of fibers that ascends or descends through the terminal zone and enter the gray matter. Some of these fibers project to the intermedial lateral columns to activate sympathetic presynaptic fibers. AP responses to ESCS observed in the present study are the results of compound responses in these multiple pathways. Nevertheless, controllability of AP by the BBS is ascertained by a clear linearity between ESCS and AP response in both static and dynamic relationships.

Although we have not confirmed it in the closed-loop condition, depressor response shown in the open-loop condition indicates that ESCS-mediated BBS can attenuate hypertension as well as hypotension. Because an offset ESCS rate (s_o) is applied in the absence of pressure disturbance, lowering ESCS rate would attenuate hypertension to some extent. AP in conscious animals fluctuates between hypertension and hypotension, even in a quiet position (5). The speed of AP restoration is considered sufficient to control these fluctuations.

Future step for clinical application. Clearly, the next step toward clinical application is to demonstrate the safety and the effectiveness of the ESCS-mediated BBS during orthostasis in conscious patients and animals. To study BBS in conscious animals, we have been developing an implantable hardware that enables BBS. Elaboration of such devices is mandatory for its future clinical application by searching the optimal stimulating site and condition that do not cause uncomfortable sensation and muscle twitch. A control algorithm must be developed that overcomes the problem revealed in the present study. The developing implant would be as small and low power as a pacemaker, with the aid of recent LSI technologies, and would be telemetrically programmable. In parallel, we began collaboration with a clinical group to develop ESCS-mediated BBS to suppress sudden hypotension in anesthetized humans during surgery. This study would prove the feasibility of human BBS.

Finally, new methods for long-term manometry are definitely required. Intravascular manometry can be achieved only with long-lasting antithrombotic material. Other indirect methods should be used until we are confident in antithrombotic ability.

Conclusions. As a step toward clinical application of BBS, we demonstrated that AP could be controlled with ESCS. We designed the artificial vasomotor center based on the dynamic characteristics of AP response to ESCS. Although there was a dissociation between the predicted and actual attenuation of AP fall, ESCS-mediated BBS with appropriate gain adjustment was capable of preventing HUT-induced hypotension rapidly, sufficiently, and stably.

APPENDIX

Simulation of AP Restoration and Implementation by the Artificial Vasomotor Center

We modeled the vasomotor center transfer function (G_c) as

$$G_c(f) = K_c \frac{1 + \frac{f}{f_{c1}}j}{\left(1 + \frac{f}{f_{c2}}j\right)\left(1 + \frac{f}{f_{c3}}j\right)} \exp(-2\pi f j L_c) \qquad (A1)$$

where f is frequency, K_c is the steady-state gain of the artificial vasomotor center, f_{c1} is f_c for derivative characteristics, f_{c2} and f_{c3} are corner frequencies for high-cut characteristics, j is an imaginary unit, and L_c is a pure delay. The value f_{c2} was set to $10 \times f_{c1}$, and f_{c3} was set to 1 Hz. These settings attenuate AP pulsation and preserve total baroreflex gain (13). L_c was introduced to simulate the possible time delay of 0.1 s in transforming AP to ESCS rate but was excluded in real-time application to improve AP stability.

The simulation was performed as follows. The block diagram in Fig. 4*A* is represented as

$$AP = G_p \cdot ESCS + P_d$$

$$ESCS = G_c \cdot AP$$

where G_p is transfer function of the peripheral effectors, and P_d is pressure disturbance to AP. Rearranging these formula yields

$$AP = G_c \cdot G_p \cdot AP + P_d \qquad (A2)$$

The time domain representation of *Eq. A2* is

$$\Delta AP(t) = \int g(\tau) \cdot \Delta AP(t - \tau)d\tau + P_d(t) \qquad (A3)$$

where $\Delta AP(t)$ is AP change from control value, and $g(\tau)$ is the impulse response function of the total open-loop transfer function ($G_c \cdot G_p$). To simulate orthostatic hypotension, $P_d(t)$ is set as an exponential AP fall to -60 mmHg with a time constant of 5 s rather than a stepwise fall (see Fig. 6*A*, *top*). We simulated the transient AP response to depressor stimulus while changing f_{c1} in the presence of the negative feedback system.

To implement the designed vasomotor center transfer function, we programmed the artificial vasomotor center to calculate ESCS rate in response to AP changes, according to the following equation:

$$ESCS(t) = \int h(\tau) \cdot \Delta AP(t - \tau)d\tau + s_o$$

where $h(\tau)$ is the impulse response function of the designed vasomotor center transfer function, $\Delta AP(t)$ is AP change from the control value, and s_o is the offset ESCS rate obtained from the static parameterization.

GRANTS

This study was supported by a Grant-in-Aid for Scientific Research (A15200040) from the Japan Society for the Promotion of Science, the Program for Promotion of Fundamental Studies in Health Science of Pharmaceuticals and Medical Devices Agency of Japan, and a Health and Labour Sciences Research Grant (Research on Advanced Medical Technology, H14-nano-002) from the Ministry of Health, Labour and Welfare of Japan.

REFERENCES

1. **Bannister R, da Costa DF, Hendry WG, Jacobs J, and Mathias CJ.** Atrial demand pacing to protect against vagal overactivity in sympathetic autonomic neuropathy. *Brain* 109: 345–356, 1986.

2. **Biaggioni I, Robertson RM, and Robertson D.** Manipulation of norepinephrine metabolism with yohimbine in the treatment of autonomic failure. *J Clin Pharmacol* 34: 418–423, 1994.
3. **Chobanian AV, Volicer L, Tifft CP, Gavras H, Liang CS, and Faxon D.** Mineralocorticoid-induced hypertension in patients with orthostatic hypotension. *N Engl J Med* 301: 68–73, 1994.
4. **Chung JM and Wurster RD.** Ascending pressor and depressor pathways in the cat spinal cord. *Am J Physiol* 231: 786–792, 1976.
5. **Cowley AW Jr, Liard JF, and Guyton AC.** Role of baroreceptor reflex in daily control of arterial blood pressure and other variables in dogs. *Circ Res* 32: 564–576, 1973.
6. **Di Pede F, Lanza GA, Zuin G, Alfieri O, Rapati M, Romano M, Circo A, Cardano P, Bellocci F, Santini M, and Maseri A; Investigators of the Prospective Italian Registry of SCS for Angina Pectoris.** Immediate and long-term clinical outcome after spinal cord stimulation for refractory stable angina pectoris. *Am J Cardiol* 91: 951–955, 2003.
7. **Frankel HL and Mathias CJ.** Severe hypertension in patients with high spinal cord lesions undergoing electro-ejaculation–management with prostaglandin E2. *Paraplegia* 18: 293–299, 1980.
8. **Glantz SA.** *Primer of Biostatistics* (4th ed.). New York: McGraw-Hill, 1997.
9. **Guyton AC, Coleman TG, and Granger HJ.** Circulation: overall regulation. *Annu Rev Physiol* 34: 13–46, 1972.
10. **Ikeda Y, Kawada T, Sugimachi M, Kawaguchi O, Shishido T, Sato T, Miyano H, Matsuura W, Alexander J Jr, and Sunagawa K.** Neural arc of baroreflex optimizes dynamic pressure regulation in achieving both stability and quickness. *Am J Physiol Heart Circ Physiol* 271: H882–H890, 1996.
11. **Illert M and Gabriel M.** Descending pathways in the cervical cord of cats affecting blood pressure and sympathetic activity. *Pflügers Arch* 335: 109–124, 1972.
12. **Kachi T, Iwase S, Mano T, Saito M, Kunimoto M, and Sobue I.** Effect of L-threo-3,4-dihydroxyphenylserine on muscle sympathetic nerve activities in Shy-Drager syndrome. *Neurology* 38: 1091–1094, 1988.
13. **Kawada T, Zheng C, Yanagiya Y, Uemura K, Miyamoto T, Inagaki M, Shishido T, Sugimachi M, and Sunagawa K.** High-cut characteristics of the baroreflex neural arc preserve baroreflex gain against pulsatile pressure. *Am J Physiol Heart Circ Physiol* 282: H1149–H1156, 2002.
14. **Kristinsson A.** Programmed atrial pacing for orthostatic hypotension. *Acta Med Scand* 214: 79–83, 1983.
15. **Malliani A, Pagani M, Lombardi F, and Cerutti S.** Cardiovascular neural regulation explored in the frequency domain. *Circulation* 84: 482–492, 1991.
16. **Marmarelis PZ and Marmarelis VZ.** *Analysis of Physiological Systems: The White-Noise Approach.* New York: Plenum, 1978.
17. **Matthews JM, Wheeler GD, Burnham RS, Malone LA, and Steadward RD.** The effects of surface anaesthesia on the autonomic dysreflexia response during functional electrical stimulation. *Spinal Cord* 35: 647–651, 1997.
18. **Meglio M, Cioni B, Rossi GF, Sandric S, and Santarelli P.** Spinal cord stimulation affects the central mechanisms of regulation of heart rate. *Appl Neurophysiol* 49: 139–146, 1986.
19. **Mehlsen J and Boesen F.** Substantial effect of acute hydration on blood pressure in patients with autonomic failure. *Clin Physiol* 7: 243–246, 1987.
20. **Obara A, Yamashita H, Onodera S, Yahara O, Honda H, and Hasebe N.** Effect of xamoterol in Shy-Drager syndrome. *Circulation* 85: 606–611, 1992.
21. **Parikh SM, Diedrich A, Biaggioni I, and Robertson D.** The nature of the autonomic dysfunction in multiple system atrophy. *J Neurol Sci* 200: 1–10, 2002.
22. **Robertson D.** Diagnosis and management of baroreflex failure. *Primary Cardiol* 21: 37–40, 1995.
23. **Sato T, Kawada T, Inagaki M, Shishido T, Takaki H, Sugimachi M, and Sunagawa K.** New analytic framework for understanding sympathetic baroreflex control of arterial pressure. *Am J Physiol Heart Circ Physiol* 276: H2251–H2261, 1999.
24. **Sato T, Kawada T, Shishido T, Sugimachi M, Alexander J Jr, and Sunagawa K.** Novel therapeutic strategy against central baroreflex failure: a bionic baroreflex system. *Circulation* 100: 299–304, 1999.
25. **Sato T, Kawada T, Inagaki M, Shishido T, Sugimachi M, and Sunagawa K.** Dynamics of sympathetic baroreflex control of arterial pressure in rats. *Am J Physiol Regul Integr Comp Physiol* 285: R262–R270, 2003.
26. **Sato T, Kawada T, Sugimachi M, and Sunagawa K.** Bionic technology revitalizes native baroreflex function in rats with baroreflex failure. *Circulation* 106: 730–734, 2002.
27. **Schramm LP and Livingston RH.** Inhibition of renal nerve sympathetic activity by spinal stimulation in rat. *Am J Physiol Regul Integr Comp Physiol* 252: R514–R525, 1987.
28. **Shannon JR, Diedrich A, Biaggioni I, Tank J, Robertson RM, Robertson D, and Jordan J.** Water drinking as a treatment for orthostatic syndromes. *Am J Med* 112: 355–360, 2002.
29. **Shimoji K, Hokari T, Kano T, Tomita M, Kimura R, Watanabe S, Endoh H, Fukuda S, Fujiwara N, and Aida S.** Management of intractable pain with percutaneous epidural spinal cord stimulation: differences in pain-relieving effects among diseases and sites of pain. *Anesth Analg* 77: 110–116, 1993.
30. **Shy M and Drager GA.** A neurological syndrome associated with orthostatic hypotension: a clinico-pathologic study. *Arch Neurol* 2: 511–527, 1960.
31. **Sugimachi M, Imaizumi T, Sunagawa K, Hirooka Y, Todaka K, Takeshita A, and Nakamura M.** A new method to identify dynamic transduction properties of aortic baroreceptors. *Am J Physiol Heart Circ Physiol* 258: H887–H895, 1990.
32. **Taylor RF and Schramm LP.** Spinally mediated inhibition of abdominal and lumbar sympathetic activities. *Am J Physiol Regul Integr Comp Physiol* 254: R655–R658, 1988.
33. **Wilcox CS, Puritz R, Lightman SL, Bannister R, and Aminoff MJ.** Plasma volume regulation in patients with progressive autonomic failure during changes in salt intake or posture. *J Lab Clin Med* 104: 331–339, 1984.

Am J Physiol Heart Circ Physiol 287: H860–H865, 2004.
First published March 11, 2004; 10.1152/ajpheart.00752.2003.

Cardiac sympathetic nerve stimulation does not attenuate dynamic vagal control of heart rate via α-adrenergic mechanism

Tadayoshi Miyamoto,[1,2] Toru Kawada,[1] Yusuke Yanagiya,[1,3] Masashi Inagaki,[1] Hiroshi Takaki,[1] Masaru Sugimachi,[1] and Kenji Sunagawa[1]

[1]*Department of Cardiovascular Dynamics, National Cardiovascular Center Research Institute, Osaka 565-8565;* [2]*Japan Association for the Advancement of Medical Equipment, Tokyo 105-0013; and* [3]*The Organization for Pharmaceutical Safety and Research, Tokyo 100-0013, Japan*

Submitted 7 August 2003; accepted in final form 6 March 2004

Miyamoto, Tadayoshi, Toru Kawada, Yusuke Yanagiya, Masashi Inagaki, Hiroshi Takaki, Masaru Sugimachi, and Kenji Sunagawa. Cardiac sympathetic nerve stimulation does not attenuate dynamic vagal control of heart rate via α-adrenergic mechanism. *Am J Physiol Heart Circ Physiol* 287: H860–H865, 2004. First published March 11, 2004; 10.1152/ajpheart.00752.2003.—Complex sympathovagal interactions govern heart rate (HR). Activation of the postjunctional β-adrenergic receptors on the sinus nodal cells augments the HR response to vagal stimulation, whereas exogenous activation of the presynaptic α-adrenergic receptors on the vagal nerve terminals attenuates vagal control of HR. Whether the α-adrenergic mechanism associated with cardiac postganglionic sympathetic nerve activation plays a significant role in modulation of the dynamic vagal control of HR remains unknown. The right vagal nerve was stimulated in seven anesthetized rabbits that had undergone sinoaortic denervation and vagotomy according to a binary white-noise signal (0–10 Hz) for 10 min; subsequently, the transfer function from vagal stimulation to HR was estimated. The effects of β-adrenergic blockade with propranolol (1 mg/kg iv) and the combined effects of β-adrenergic blockade and tonic cardiac sympathetic nerve stimulation at 5 Hz were examined. The transfer function from vagal stimulation to HR approximated a first-order, low-pass filter with pure delay. β-Adrenergic blockade decreased the dynamic gain from 6.0 ± 0.4 to 3.7 ± 0.6 beats·min^{-1}·Hz^{-1} ($P < 0.01$) with no alteration of the corner frequency or pure delay. Under β-adrenergic blockade conditions, tonic sympathetic stimulation did not further change the dynamic gain (3.8 ± 0.5 beats·min^{-1}·Hz^{-1}). In conclusion, cardiac postganglionic sympathetic nerve stimulation did not affect the dynamic HR response to vagal stimulation via the α-adrenergic mechanism.

systems analysis; transfer function; β-adrenergic blockade; rabbits; sympathovagal interaction

COMPLEX SYMPATHOVAGAL INTERACTIONS are known to occur in the regulation of heart rate (HR). These interactions involve neural interactions within and between cardiac ganglia (2, 3), at the end terminals for their cardiac projections (18), and via second-messenger systems in the innervated myocytes (29). An increase in background sympathetic tone augments the HR response to vagal nerve activity (19, 20). Levy (19) referred to this phenomenon as an accentuated antagonism of HR control. Accumulation of cAMP in the sinus nodal cells via activation of postjunctional β-adrenergic receptors contributed to the accentuated antagonism (25). On the other hand, activation of the prejunctional α-adrenergic receptors attenuated ACh release from the cardiac vagal nerve terminals (1, 22, 23, 26–28, 30, 31). Akiyama et al. (1) demonstrated that local norepinephrine (NE) administration in the feline heart attenuated myocardial interstitial ACh release during electrical vagal stimulation via the α-adrenergic mechanism. These findings, in concert, indicate that whether the HR response to vagal stimulation is augmented or attenuated by concomitant sympathetic tone depends on the type and site of adrenergic receptors most selectively activated under a given condition.

Our previous studies performed on the rabbit indicated that elevated cardiac sympathetic nerve activity augmented the dynamic HR response to vagal nerve stimulation via activation of the postjunctional β-adrenergic cascade (13, 14, 25). On the other hand, high plasma NE levels attenuated the dynamic HR response to vagal stimulation via the α-adrenergic mechanism (24). However, whether NE released from cardiac postganglionic sympathetic nerve terminals exerts presynaptic inhibition on vagal control of HR via the α-adrenergic mechanism remains unknown. We hypothesized that cardiac postganglionic sympathetic nerve stimulation under β-adrenergic blockade conditions would manifest, if any, the presynaptic inhibition on vagal control of HR. The objective of the present investigation was therefore to examine the effects of tonic sympathetic nerve stimulation on the dynamic vagal control of HR under β-adrenergic blockade conditions. The results indicated that cardiac postganglionic sympathetic nerve stimulation did not affect the dynamic HR response to vagal stimulation via the α-adrenergic mechanism.

MATERIALS AND METHODS

Surgical preparations. Animal care was in accordance with "Guiding Principles for the Care and Use of Animals in the Field of Physiological Sciences," which was approved by the Physiological Society of Japan. Twelve Japanese White rabbits (body wt, 2.5–3.1 kg) were anesthetized via injection (2 ml/kg iv) of a mixture of urethane (250 mg/ml) and α-chloralose (40 mg/ml); subsequently, the rabbits were mechanically ventilated with oxygen-enriched room air. Supplemental doses of these anesthetics were administered as necessary via the marginal ear vein. Aortic pressure (AP) was monitored with a micromanometer catheter (Millar Instruments; Houston, TX) inserted via the right femoral artery. A catheter for drug administration was inserted into the right femoral vein. Sinoaortic denervation was performed bilaterally to minimize changes in sympathetic efferent nerve activity via the arterial baroreflexes. The vagi were sectioned bilaterally at the neck. A pair of bipolar platinum electrodes

Address for reprint requests and other correspondence: T. Miyamoto, Dept. of Cardiovascular Dynamics, National Cardiovascular Center Research Institute, 5-7-1 Fujishirodai, Suita, Osaka 565-8565, Japan (E-mail: miyamoto@res.ncvc.go.jp).

The costs of publication of this article were defrayed in part by the payment of page charges. The article must therefore be hereby marked "*advertisement*" in accordance with 18 U.S.C. Section 1734 solely to indicate this fact.

was then attached to the cardiac end of the sectioned right vagus for dynamic vagal stimulation. The right inferior cardiac sympathetic nerve, which mainly consists of postganglionic nerve fibers in the rabbit (15), was exposed through a midline thoracotomy. A second pair of bipolar platinum electrodes was attached for tonic sympathetic nerve stimulation. To prevent drying and provide insulation, the stimulation electrodes and the nerves were immersed in a mixture of white petroleum jelly (Vaseline) and liquid paraffin. Instantaneous HR was measured from the AP signal utilizing a cardiotachometer (model N4778, San-ei). Body temperature was maintained at 38°C with a heating pad throughout the experiment.

Protocols. The pulse duration of nerve stimulation was set at 2 ms. The stimulation amplitude of the right vagus was adjusted to yield a HR decrease of ~50 beats/min at a stimulation frequency of 5 Hz. After adjustment, the amplitude of vagal stimulation ranged from 3.5 to 6.0 V. The stimulation amplitude of the right cardiac postganglionic sympathetic nerve was adjusted to yield a HR increase of 50 beats/min at a stimulation frequency of 5 Hz. After adjustment, the amplitude of sympathetic stimulation ranged from 1.8 to 3.8 V.

In *protocol 1* (n = 7), which was done to estimate the transfer function from vagal stimulation to HR response, the right vagus was stimulated employing a frequency-modulated pulse train. The stimulation frequency was switched every second at either 0 or 10 Hz according to a binary white-noise signal. The power spectrum of the stimulation signal, which was reasonably constant up to 0.5 Hz, decreased gradually to 1/10 at ~0.8 Hz and diminished sharply as the frequency increased to 1 Hz. The transfer function was estimated only up to 0.8 Hz, because the reliability of estimation decreased due to the lack of input power above this frequency. The selected frequency range sufficiently spanned the physiological range of interest with respect to dynamic vagal control of HR in rabbits (13, 14, 24, 25).

The transfer function from dynamic vagal stimulation to the HR response was estimated from 10-min data under the following three conditions: control, β-adrenergic blockade, and β-adrenergic blockade plus tonic sympathetic nerve stimulation. After the control data was recorded, a bolus injection of propranolol (1 mg/kg iv) was administered; ~10 min elapsed before HR and AP reached the new steady state. Under β-adrenergic blockade conditions, estimation of the transfer function was repeated with and without simultaneous 5-Hz tonic sympathetic stimulation. The order of the latter two conditions was randomized across the animals. The control data was obtained first in all animals, as the long-lasting effects of propranolol did not permit the subsequent acquisition of control data.

In *protocol 2* (n = 5), which was done to examine the stability of electrical sympathetic stimulation, 1-min stimulation of the right cardiac postganglionic sympathetic nerve was repeated every 10 min for 6 stimulations.

Data analysis. Data were digitized at 200 Hz utilizing a 12-bit analog-to-digital converter and stored on the hard disk of a dedicated laboratory computer system.

In *protocol 1*, prestimulation values for HR and AP were obtained by averaging the respective data for 10 s immediately before vagal stimulation in each condition. Mean values for HR and AP during vagal stimulation were calculated by averaging the respective data over the time period of dynamic vagal stimulation.

The transfer function from dynamic vagal stimulation to the HR response was estimated based on the following procedure. Input-output data pairs of the vagal stimulation frequency and HR were resampled at 10 Hz; subsequently, data pairs were partitioned into eight 50%-overlapping segments consisting of 1,024 data points each. For each segment, the linear trend was subtracted and a Hanning window was applied. A fast Fourier transform was then performed to obtain the frequency spectra for vagal stimulation [$N(f)$] and HR [HR(f)] (7). Over the eight segments, the power of the vagal stimulation [$S_{N\cdot N}(f)$], that of HR [$S_{HR\cdot HR}(f)$], and the cross-power between these two signals [$S_{N\cdot HR}(f)$] were ensemble averaged. Finally, the transfer function [H(f)] from vagal stimulation to HR response was determined using the following equation (4, 21)

$$H(f) = \frac{S_{N\cdot HR}(f)}{S_{N\cdot N}(f)}$$

The transfer function from vagal stimulation to HR response approximated a first-order, low-pass filter with pure delay in previous studies (13, 14, 24, 25); therefore, the estimated transfer function was parameterized with the equation

$$H(f) = \frac{-K}{1 + \frac{f}{f_C} j} e^{-2\pi f j L}$$

where K represents dynamic gain (in beats·min^{-1}·Hz^{-1}), f_C denotes corner frequency (in Hz), L denotes pure delay (in s), and f and j represent frequency and an imaginary unit, respectively. The negative sign in the numerator indicates the negative HR response to vagal stimulation. The parameters were estimated by means of iterative nonlinear least-squares regression.

To quantify the linear dependence of the HR response on vagal

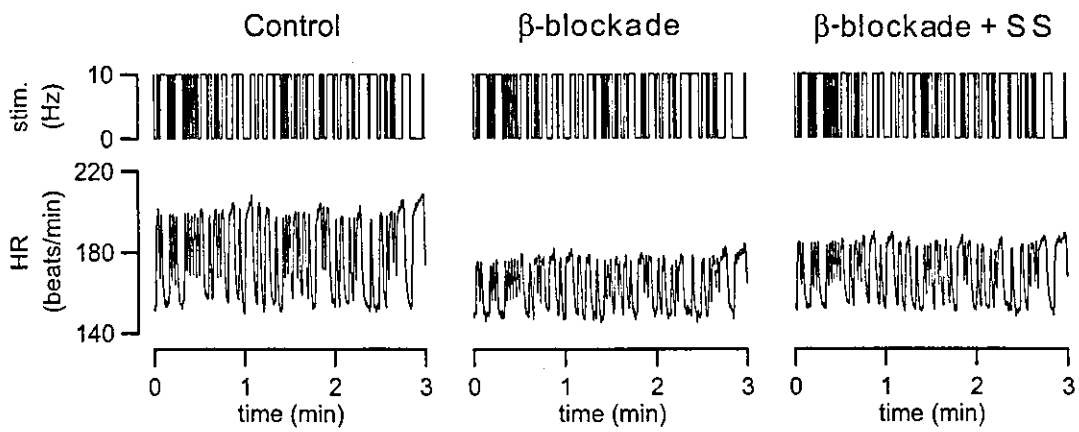

Fig. 1. Representative recordings of vagal stimulation (stim) obtained utilizing a binary white-noise signal (*top*) and the corresponding heart rate (HR) responses (*bottom*). Recordings before (Control; *left*) and after infusion of β-adrenergic blockade with propranolol (1 mg/kg iv; *middle*) and β-adrenergic blockade plus tonic sympathetic nerve stimulation (β-blockade + SS; *right*) are shown. β-Adrenergic blockade decreased mean HR and attenuated the amplitude of HR variation. Tonic sympathetic nerve stimulation concomitant with the β-adrenergic blockade did not further affect the amplitude of HR variation.

Table 1. *Mean heart rate and aortic pressure values before and during vagal stimulation obtained from protocol 1*

	Control	β-Blockade	β-Blockade + SS
Heart rate, beats/min			
Prestimulation	243±19	206±12*	204±11*
During stimulation	208±16	185±12**	184±12**
Aortic pressure, mmHg			
Prestimulation	103±6	90±6	89±9
During stimulation	101±7	88±6	89±7

Values are means ± SE. β-Blockade, β-adrenergic blockade with propranolol (1 mg/kg iv); β-blockade + SS, β-adrenergic blockade with propranolol and constant cardiac sympathetic stimulation at 5 Hz. *$P < 0.01$; **$P < 0.05$ vs. corresponding control.

stimulation, the magnitude-squared coherence function [Coh(f)] was estimated employing the equation (4, 21)

$$\mathrm{Coh}(f) = \frac{|S_{N\cdot HR}(f)|^2}{S_{N\cdot N}(f) \cdot S_{HR\cdot HR}(f)}$$

Coherence value ranges from zero to unity. Unity coherence indicates perfect linear dependence between the input and output signals; in contrast, zero coherence indicates total independence between the two signals.

In *protocol 2*, prestimulation values of HR and AP were obtained by averaging the respective data for 10 s immediately before each 1-min sympathetic stimulation. The steady-state HR value was obtained by averaging instantaneous HR data for the last 10 s of each 1-min sympathetic stimulation. The HR increase at each sympathetic stimulation was calculated from the difference between the steady-state and prestimulation HR values.

Statistics. All data are presented as means ± SE. In *protocol 1*, the mean levels of HR and AP and fitted parameters of the transfer function were compared among conditions of control, β-adrenergic blockade, and β-adrenergic blockade plus tonic sympathetic stimulation by repeated-measures ANOVA. When a significant difference ($P < 0.05$) was evident among the three conditions, Tukey's test for all pairwise comparisons (9) was applied to identify the inequality between the two conditions with a significance level of $P < 0.05$.

RESULTS

Figure 1 exhibits typical recordings of vagal stimulation and HR response under conditions of control, β-adrenergic blockade, and β-adrenergic blockade plus tonic sympathetic nerve stimulation. Random vagal stimulation decreased HR intermittently. β-Adrenergic blockade decreased mean HR and attenuated the amplitude of HR variation. Tonic sympathetic nerve stimulation in the presence of the β-adrenergic blockade did not further affect the amplitude of HR variation. The speed of the response of HR to vagal stimulation appeared to be unchanged across the three conditions.

Table 1 summarizes prestimulation and mean values of HR and AP during vagal stimulation averaged from all animals in *protocol 1*. β-Adrenergic blockade significantly decreased prestimulation and mean values of HR during vagal stimulation. Tonic sympathetic nerve stimulation did not alter prestimulation and mean values of HR compared with the β-adrenergic blockade conditions. Changes in AP were not statistically significant.

Figure 2 illustrates the transfer functions from vagal stimulation to the HR response averaged from all animals in *protocol 1*. The gain plots, phase plots, and coherence functions are shown. The transfer gain was relatively constant below 0.05 Hz and decreased above 0.05 Hz up to 0.8 Hz in each panel. The phase approached $-\pi$ radians at the lowest frequency and lagged with increasing frequency. Coherence was near unity in the frequency range below 0.5 Hz under control conditions. A slight decrease from unity in the coherence values was noted under β-adrenergic blockade conditions with and without tonic sympathetic nerve stimulation.

The fitted parameters of the transfer functions are summarized in Table 2. β-Adrenergic blockade decreased dynamic gain with no alteration of the corner frequency or pure delay. Under β-adrenergic blockade conditions, tonic sympathetic nerve stimulation did not further change the dynamic gain.

Table 3 shows the prestimulation values of HR and AP and the HR increase in response to tonic sympathetic nerve

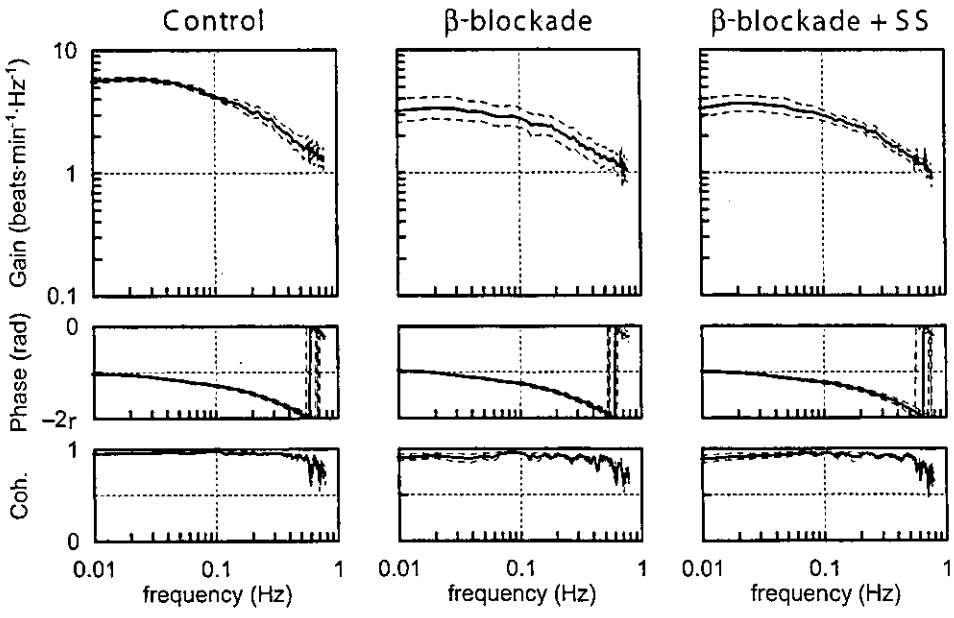

Fig. 2. Transfer functions from vagal stimulation to the HR response averaged from all animals ($n = 7$), and right panels display transfer functions before (*left*) and after (*middle*) infusion of propranolol in the absence and presence (*right*) of SS are shown. Gains (*top*), phase shifts (*middle*), and coherence functions (Coh; *bottom*) are presented. Solid lines represent the means, whereas dashed lines indicate means ± SE values. Transfer gain was relatively constant below 0.05 Hz; furthermore, it decreased above this frequency up to 0.8 Hz in each panel. β-Adrenergic blockade decreased the gain of the transfer function. SS under β-adrenergic blockade conditions did not alter the gain of the transfer function compared with β-adrenergic blockade conditions.

Table 2. *Parameters of transfer function from vagal stimulation to heart rate response*

	Control	β-Blockade	β-Blockade + SS
Dynamic gain, beats·min^{-1}·Hz^{-1}	6.0±0.4	3.7±0.6*	3.8±0.5*
Corner frequency, Hz	0.19±0.06	0.22±0.04	0.24±0.04
Pure delay, s	0.49±0.05	0.55±0.07	0.45±0.03

Values are means ± SE. *$P < 0.05$ vs. corresponding control values.

stimulation obtained from *protocol 2*. The HR increase to tonic sympathetic nerve stimulation did not change significantly for 50 min, which covered the entire time period of *protocol 1*.

DISCUSSION

We have demonstrated that β-adrenergic blockade with intravenous propranolol administration decreased the dynamic gain of the transfer function from vagal stimulation to HR. Under β-adrenergic blockade conditions, tonic stimulation of the cardiac postganglionic sympathetic nerve did not affect the dynamic gain of the HR response to vagal stimulation.

Effects of tonic sympathetic nerve stimulation on dynamic vagal control of HR under β-adrenergic blockade conditions. Previous studies indicate that activation of α-adrenergic receptors modulates the vagal control of HR. Pardini et al. (26) showed that α-adrenergic stimulation by intravenous phenylephrine inhibited the HR response to electrical stimulation of the preganglionic vagal fibers, whereas this treatment facilitated the HR response to carbachol-induced activation of the postganglionic vagal fibers. In a previous investigation (24), we demonstrated that intravenous NE infusion attenuated dynamic vagal control of HR via the α-adrenergic mechanism. However, because these previous studies employed phenylephrine or NE administration, whether endogenous NE released from the cardiac sympathetic nerve terminals modulated the vagal control of HR via the α-adrenergic mechanism remained unknown.

In the present investigation, the effects of electrical stimulation of the cardiac postganglionic sympathetic nerve on vagal control of HR were examined under β-adrenergic blockade conditions. Selective stimulation of the cardiac sympathetic nerve did not increase plasma NE concentration perceivably (8, 16, 32). Therefore, changes in the vagal control of HR, if any, could be attributable to the effects of NE released from the postganglionic cardiac sympathetic nerve terminals. As depicted in Fig. 2, dynamic vagal control of HR was unaffected by tonic sympathetic nerve stimulation under β-adrenergic blockade conditions, which suggests that modulation of the vagal control of HR via the α-adrenergic mechanism is negligible during selective stimulation of the cardiac sympathetic nerve. A failure to stimulate the sympathetic nerve cannot account for this observation, because the HR response to sympathetic nerve stimulation was reproducible in *protocol 2* for the time period necessary for completing *protocol 1* (see Table 3).

In addition to classical nicotinic cholinergic synapses, β-adrenergic synapses are present in sympathetic ganglia (3). Hence, β-adrenergic blockade can alter sympathetic transmission in the intrathoracic cardiac nervous system. However, because the right inferior sympathetic nerve we stimulated was mainly postganglionic in rabbits (15), the lack of sympathetic effects after β-adrenergic blockade cannot be ascribed to the interruption of sympathetic ganglionic transmission to the heart. Another factor that should be taken into account is the extent of overlap in innervation between the sympathetic and vagal systems. If the innervation does not overlap at all, NE released from the sympathetic nerve terminals may not reach the prejunctional α-adrenergic receptors on the vagal nerve terminals. However, we stimulated right-sided inputs for both parasympathetic and sympathetic inputs and thereby maximized the potential of neural interactions. Under similar experimental conditions, we detected sympathovagal interactions in the absence of β-adrenergic blockade in previous studies (13, 14). Therefore, we speculate that there was substantial overlap in innervation between the nerves we were activating.

Effects of β-adrenergic blockade on dynamic vagal control of HR. The present results indicated that β-adrenergic blockade significantly attenuated the dynamic gain of the vagal control of HR (see Fig. 2). These results are consistent with findings in a previous study on dogs (6). β-Adrenergic blockade decreased mean HR during dynamic vagal stimulation (see Table 1), which suggests that a considerable sympathetic tone had existed under control conditions. Although the right inferior cardiac sympathetic nerve was sectioned, other sympathetic branches directed to the heart were kept intact and may have provided sympathetic tone under control conditions. The withdrawal of such background sympathetic tone after β-adrenergic blockade reduced the dynamic gain of the vagal control of HR.

Plasma catecholamines also participate in the background sympathetic tone. Although we demonstrated that high plasma NE concentration attenuated dynamic vagal control of HR (24), the effects of plasma epinephrine on dynamic vagal control of HR remain unknown. It is possible that plasma epinephrine exerted a positive chronotropic effect and augmented dynamic vagal control of HR under control conditions. However, previous studies using cardiac microdialysis have indicated that plasma catecholamines can dissociate from myocardial interstitial catecholamine levels due to substantial compartmentalization (16, 18). Myocardial interstitial NE levels correlate with left ventricular contractility regardless of

Table 3. *Effects of cardiac sympathetic stimulation on heart rate response obtained from protocol 2*

	Time, min					
	1	11	21	31	41	51
ΔHR, beats/min	49.9±7.0	51.0±5.5	49.1±3.4	43.5±3.7	45.0±4.6	45.4±5.1
Prestimulation HR, beats/min	240.9±13.2	238.3±12.9	234.8±11.3	235.3±11.8	231.8±11.7	232.1±12.7
Prestimulation AP, mmHg	88.2±8.7	86.5±8.5	82.7±8.7	85.1±9.1	86.0±9.4	87.7±9.0

Values are means ± SE. HR, heart rate; AP, aortic pressure.

whether the interstitial NE levels were increased endogenously with cardiac sympathetic stimulation or exogenously with intravenous NE infusion (16). Therefore, not only plasma but also myocardial interstitial catecholamine levels are important for determining cardiac function. Additional studies are necessary to determine whether high levels of plasma and/or myocardial interstitial epinephrine modulate the dynamic vagal control of HR.

Limitations. First, data were obtained from animals under anesthetized conditions. In the event that data had been obtained from conscious animals, the results may have been different. However, because we stimulated the efferent pathways of the sectioned vagal and cardiac sympathetic nerves, the effects of anesthesia on the central nervous system may not influence the present results much. Furthermore, because we compared the vagal control of HR among the three different conditions under the same anesthesia, it is fair to say that the tonic sympathetic stimulation did not affect the vagal control of HR via the α-adrenergic mechanism.

Second, rabbits may exhibit a different degree of sympathovagal interaction compared with the more commonly studied dogs. However, the HR response to autonomic nerve stimulation is similar between rabbits and dogs in various aspects. The HR response to vagal stimulation is faster than that to sympathetic stimulation (5, 13). The accentuated antagonism (10, 19) and presynaptic inhibition (11, 28) between the vagal and sympathetic nerves were observed in both species. The three-dimensional plot derived from the steady-state HR response to various combinations of vagal and sympathetic stimulation is similar for the two species (14, 19). We therefore believe that rabbits are as good as dogs for investigating the autonomic control of HR.

Finally, the stimulation pattern of binary white noise differs from the physiological discharge of the vagal nerve (17). Notably, the aphasic nature of binary white-noise stimulation relative to each R-R interval would mask the phase-dependent sensitivity of the HR response to nerve stimulation (12). Moreover, we stimulated the entire bundle of the vagal nerve simultaneously. Thus the dynamic HR response determined in the present study cannot account for possible regional differences in nerve function among the nerve fibers.

In conclusion, cardiac postganglionic sympathetic nerve stimulation did not affect the dynamic HR response to vagal stimulation via the α-adrenergic mechanism in rabbits. Presynaptic inhibition of the vagal control of HR might manifest itself upon activation of the presynaptic α-adrenergic receptors on the preganglionic and/or postganglionic vagal nerve terminals by circulatory agents.

GRANTS

This study was supported by Research Grants for Cardiovascular Diseases (11C-3 and 11C-7) from the Ministry of Health and Welfare of Japan; by a Health Sciences Research Grant for Advanced Medical Technology from the Ministry of Health and Welfare of Japan; by a Grant-in-Aid for Scientific Research (B-11694337, C-11680862, and C-11670730) and a Grant-in-Aid for Encouragement of Young Scientists (13770378) from the Ministry of Education, Science, Sports, and Culture of Japan; by Japan Science and Technology Research and Development for Applying Advanced Computational Science and Technology; and by the Program for Promotion of Fundamental Studies in Health Science from the Organization for Pharmaceutical Safety and Research.

REFERENCES

1. **Akiyama T and Yamazaki T.** Adrenergic inhibition of endogenous acetylcholine release on postganglionic cardiac vagal nerve terminals. *Cardiovasc Res* 46: 531–538, 2000.
2. **Armour JA.** Peripheral autonomic neuronal interactions in cardiac regulation. In: *Neurocardiology*, edited by Armour JA and Ardell JL. New York: Oxford University Press, 1994, p. 219–244.
3. **Armour JA and Butler CK.** Intrathoracic ganglionic beta-adrenergic receptors involved in efferent sympathetic regulation of the canine heart. *Can J Cardiol* 5: 275–283, 1989.
4. **Bendat JS and Piersol AG.** Single-input/output relationships. In: *Random Data Analysis and Measurement Procedures* (3rd ed). New York: Wiley, 2000, p. 189–217.
5. **Berger RD, Saul JP, and Cohen RJ.** Transfer function analysis of autonomic regulation. I. Canine atrial rate response. *Am J Physiol Heart Circ Physiol* 256: H142–H152, 1989.
6. **Bibevski S and Dunlap ME.** Ganglionic mechanisms contribute to diminished vagal control in heart failure. *Circulation* 99: 2958–2963, 1999.
7. **Brigham EO.** FFT transform applications. In: *The Fast Fourier Transform and Its Applications*. Englewood Cliffs, NJ: Prentice-Hall, 1988, p. 167–203.
8. **Ellingsen O, Vengen OA, Kjeldsen SE, Eide I, and Ilebekk A.** Myocardial potassium uptake and catecholamine release during cardiac sympathetic nerve stimulation. *Cardiovasc Res* 21: 892–901, 1987.
9. **Glantz SA.** *Primer of Biostatistics* (5th ed). New York: McGraw-Hill, 2002.
10. **Grodner AS, Lahrtz HS, Pool PE, and Braunwald E.** Neurotransmitter control of sinoatrial pacemaker frequency in isolated rat atria and in intact rabbits. *Circ Res* 27: 867–873, 1970.
11. **Habermeier-Muth A and Muscholl E.** Short- and long-latency muscarinic inhibition of noradrenaline release from rabbit atria induced by vagal stimulation. *J Physiol* 401: 277–293, 1988.
12. **Jalife J and Michaels DC.** Phase-dependent interactions of cardiac pacemakers as mechanisms of control and synchronization in the heart. In: *Cardiac Electrophysiology and Arrhythmias*, edited by Zipes DP and Jalife J. New York: Grune and Stratton, 1985, p. 109–119.
13. **Kawada T, Ikeda Y, Sugimachi M, Shishido T, Kawaguchi O, Yamazaki T, Alexander J Jr, and Sunagawa K.** Bidirectional augmentation of heart rate regulation by autonomic nervous system in rabbits. *Am J Physiol Heart Circ Physiol* 271: H288–H295, 1996.
14. **Kawada T, Sugimachi M, Shishido T, Miyano H, Sato T, Yoshimura R, Miyashita H, Nakahara T, Alexander J Jr, and Sunagawa K.** Simultaneous identification of static and dynamic vagosympathetic interactions in regulating heart rate. *Am J Physiol Regul Integr Comp Physiol* 276: R782–R789, 1999.
15. **Kawada T, Uemura K, Kashihara K, Jin Y, Li M, Zheng C, Sugimachi M, and Sunagawa K.** Uniformity in dynamic baroreflex regulation of left and right cardiac sympathetic nerve activities. *Am J Physiol Regul Integr Comp Physiol* 284: R1506–R1512, 2003.
16. **Kawada T, Yamazaki T, Akiyama T, Shishido T, Miyano H, Sato T, Sugimachi M, Alexander J Jr, and Sunagawa K.** Interstitial norepinephrine level by cardiac microdialysis correlates with ventricular contractility. *Am J Physiol Heart Circ Physiol* 273: H1107–H1112, 1997.
17. **Kollai M and Koizumi K.** Cardiovascular reflexes and interrelationships between sympathetic and parasympathetic activity. *J Auton Nerv Syst* 4: 135–148, 1981.
18. **Lameris TW, de Zeeuw S, Alberts G, Boomsma F, Duncker DJ, Verdouw PD, Veld AJ, and van Den Meiracker AH.** Time course and mechanism of myocardial catecholamine release during transient ischemia in vivo. *Circulation* 101: 2645–2650, 2000.
19. **Levy MN.** Sympathetic-parasympathetic interactions in the heart. *Circ Res* 29: 437–445, 1971.
20. **Levy MN.** Autonomic interactions in cardiac control. *Ann NY Acad Sci* 601: 209–221, 1990.
21. **Marmarelis PZ and Marmarelis VZ.** The white noise method in system identification. In: *Analysis of Physiological Systems*. New York: Plenum, 1978, p. 131–221.
22. **McDonough PM, Wetzel GT, and Brown JH.** Further characterization of the presynaptic α_1-receptor modulating [^{3}H]ACh release from rat atria. *J Pharmacol Exp Ther* 238: 612–617, 1986.

23. **McGrattan PA, Brown JH, and Brown OM.** Parasympathetic effects on in vivo rat heart can be regulated through an α_1-adrenergic receptor. *Circ Res* 60: 465–471, 1987.
24. **Miyamoto T, Kawada T, Takaki H, Inagaki M, Yanagiya Y, Jin Y, Sugimachi M, and Sunagawa K.** High plasma norepinephrine attenuates dynamic heart rate response to vagal stimulation. *Am J Physiol Heart Circ Physiol* 284: H2412–H2418, 2003.
25. **Nakahara T, Kawada T, Sugimachi M, Miyano H, Sato T, Shishido T, Yoshimura R, Miyashita H, Inagaki M, Alexander J Jr, and Sunagawa K.** Accumulation of cAMP augments dynamic vagal control of heart rate. *Am J Physiol Heart Circ Physiol* 275: H562–H567, 1998.
26. **Pardini BJ, Lund DD, and Schmid PG.** Contrasting preganglionic and postganglionic effects of phenylephrine on parasympathetic control of heart rate. *Am J Physiol Heart Circ Physiol* 260: H118–H122, 1991.
27. **Starke K.** Alpha sympathomimetic inhibition of adrenergic and cholinergic transmission in the rabbit heart. *Naunyn Schmiedebergs Arch Pharmacol* 274: 18–45, 1972.
28. **Vizi ES.** Interaction between adrenergic and cholinergic systems: presynaptic inhibitory effect of noradrenaline on acetylcholine release. *J Neural Transm Suppl* 11: 61–78, 1974.
29. **Watanabe AM, Lindemann JP, and Fleming JW.** Mechanisms of muscarinic modulation of protein phosphorylation in intact ventricles. *Fed Proc* 43: 2618–2623, 1984.
30. **Wetzel GT and Brown JH.** Presynaptic modulation of acetylcholine release from cardiac parasympathetic neurons. *Am J Physiol Heart Circ Physiol* 248: H33–H39, 1985.
31. **Wetzel GT, Goldstein D, and Brown JH.** Acetylcholine release from rat atria can be regulated through an α_1-adrenergic receptor. *Circ Res* 56: 763–766, 1985.
32. **Yamaguchi N, de Champlain J, and Nadeau R.** Correlation between the response of the heart to sympathetic stimulation and the release of endogenous catecholamines into the coronary sinus of the dog. *Circ Res* 36: 662–668, 1975.

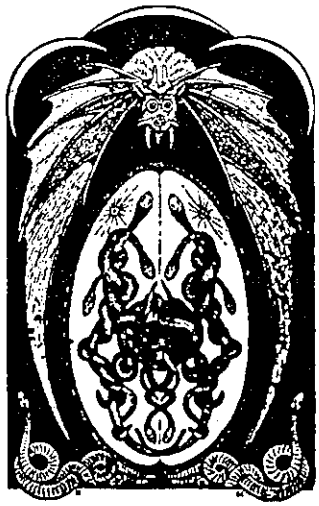

tapraid4/zh4-ahea/zh4-ahea/zh400604/zh43109d04g | moyerr | S=6 | 3/30/04 | 17:09 | MS: H0787-3 | lni: 06e/sa\dlh | Input-dms

Am J Physiol Heart Circ Physiol 286: H000–H000, 2004.
First published February 12, 2004; 10.1152/ajpheart.00787.2003.

A derivative-sigmoidal model reproduces operating point-dependent baroreflex neural arc transfer characteristics

Toru Kawada,[1] Kazunori Uemura,[1] Koji Kashihara,[1,2]
AQ: 1 **Atsunori Kamiya,[1] Masaru Sugimachi,[1] and Kenji Sunagawa[1]**
[1]*Department of Cardiovascular Dynamics, National Cardiovascular Center Research Institute,*
AQ: 2 *Osaka 565-8565; and* [2]*Organization for Pharmaceutical Safety and Research, Tokyo ???-????, Japan*

Submitted 18 August 2003; accepted in final form 9 February 2004

Kawada, Toru, Kazunori Uemura, Koji Kashihara, Atsunori Kamiya, Masaru Sugimachi, and Kenji Sunagawa. A derivative-sigmoidal model reproduces operating point-dependent baroreflex neural arc transfer characteristics. *Am J Physiol Heart Circ Physiol* 286: H000–H000, 2004. First published February 12, 2004; 10.1152/ajpheart.00787.2003.—A cascade model comprised of a derivative filter followed by a nonlinear sigmoidal component reproduces the input size dependence of transfer gain in the baroreflex neural arc from baroreceptor pressure input to efferent sympathetic nerve activity (SNA). We examined whether the same model could predict the operating point dependence of the baroreflex neural arc transfer characteristics estimated by a binary white noise input. In eight anesthetized rabbits, we isolated bilateral carotid sinuses from the systemic circulation and controlled intracarotid sinus pressure (CSP). We estimated the linear transfer function from CSP to SNA while varying mean CSP among 70, 100, 130, and 160 mmHg (P_{70}, P_{100}, P_{130}, and P_{160}, respectively). The transfer gain at 0.01 Hz was significantly smaller at P_{70} (0.61 ± 0.26) and P_{160} (0.60 ± 0.25) than at P_{100} (1.32 ± 0.42) and P_{130} (1.36 ± 0.45) (in arbitrary units/
AQ: 3 mmHg; means ± SD; $P < 0.05$). In contrast, transfer gain values above 0.5 Hz were similar among the protocols. As a result, the slope of increasing gain between 0.1 and 0.5 Hz was significantly steeper at P_{70} (17.6 ± 3.6) and P_{160} (14.1 ± 4.3) than at P_{100} (8.1 ± 4.4) and P_{130} (7.4 ± 6.6) (in dB/decade; means ± SD; $P < 0.05$). These results were consistent with those predicted by the derivative-sigmoidal model, where the deviation of mean input pressure from the center of the sigmoidal nonlinearity reduced the transfer gain mainly in the low-frequency range. The derivative-sigmoidal model functionally reproduces the dynamic SNA regulation by the arterial baroreflex over a wide operating range.

systems analysis; transfer function; simulation; carotid sinus baroreflex; nonlinearity

THE ARTERIAL BAROREFLEX SYSTEM is one of the important negative-feedback systems that stabilize arterial pressure (AP) against pressure disturbances during daily activity. A systematic analysis of baroreflex dynamic characteristics is essential for better understanding of physiological AP regulation, leading to the development of a bionic baroreflex system that can replace a failed vasomotor center (25, 26). We have analyzed the arterial baroreflex system by breaking its sympathetic limb down into neural and peripheral arc subsystems (8, 21, 24). The dynamic SNA response to baroreceptor pressure input becomes greater as the frequency of input perturbation increases in the frequency range between 0.01 and 1 Hz in anesthetized rabbits and rats (8, 15, 23), suggesting derivative characteristics of the baroreflex neural arc. In contrast, the dynamic AP response to SNA becomes smaller as the modulation frequency of SNA increases in the same frequency range, indicating the low-pass characteristics of the baroreflex peripheral arc. The fast neural arc effectively compensates for the slow peripheral arc to accelerate dynamic AP regulation by the baroreflex negative-feedback loop (8).

The static input-output relationship between baroreceptor pressure input and AP determined under open-loop conditions approximates a nonlinear sigmoidal curve with threshold and saturation (1, 2, 16, 22, 28). Under closed-loop conditions, the baroreceptor pressure input equilibrates with AP. The closed-loop operating pressure thus determined is near the center of the sigmoid curve in anesthetized rabbits and rats (4, 24). The baroreflex dynamic characteristics frequently have been estimated by using the mean input pressure around the closed-loop operating pressure (8–10, 14, 15, 19, 20). Accordingly, the baroreflex dynamic characteristics have not yet been elucidated over a wide operating range.

In a previous study, we (14) demonstrated that a cascade model consisting of a linear derivative filter followed by a nonlinear sigmoidal component (a class of Wiener model) can serve as a first approximation of neural arc transfer characteristics. Using this model, we simulated how differences in mean input pressure affect the linear transfer function from pressure input to SNA. On the basis of results of simulation using a binary white noise input, we hypothesized that deviation of the mean input pressure from the closed-loop operating pressure would decrease the neural arc transfer gain mainly in the low-frequency range, while not affecting that in the high-frequency range. To test this hypothesis, we performed an open-loop experiment on the carotid sinus baroreflex in anesthetized rabbits. The previous investigation (14) focused on developing a proper model for the overall transfer characteristics of the baroreflex neural arc based on a particular set of data, whereas the present investigation focused on verifying the model by predicting system behavior in response to input signals that had not been examined during the model construction. The results of the present study supported our hypothesis that the deviation of mean input pressure from the closed-loop operating pressure affects neural arc transfer gain in a frequency-dependent manner.

MATERIALS AND METHODS

Simulation study. Figure 1*A* illustrates a cascade model consisting F1
of a derivative filter followed by a nonlinear sigmoidal component

AQ: 7 Address for reprint requests and other correspondence: T. Kawada, Dept. of Cardiovascular Dynamics, National Cardiovascular Center Research Institute, 5-7-1 Fujishirodai, Suita-shi, Osaka 565-8565, Japan (E-mail: torukawa@res.ncvc.go.jp).

AQ: 7 The costs of publication of this article were defrayed in part by the payment of page charges. The article must therefore be hereby marked "*advertisement*" in accordance with 18 U.S.C. Section 1734 solely to indicate this fact.

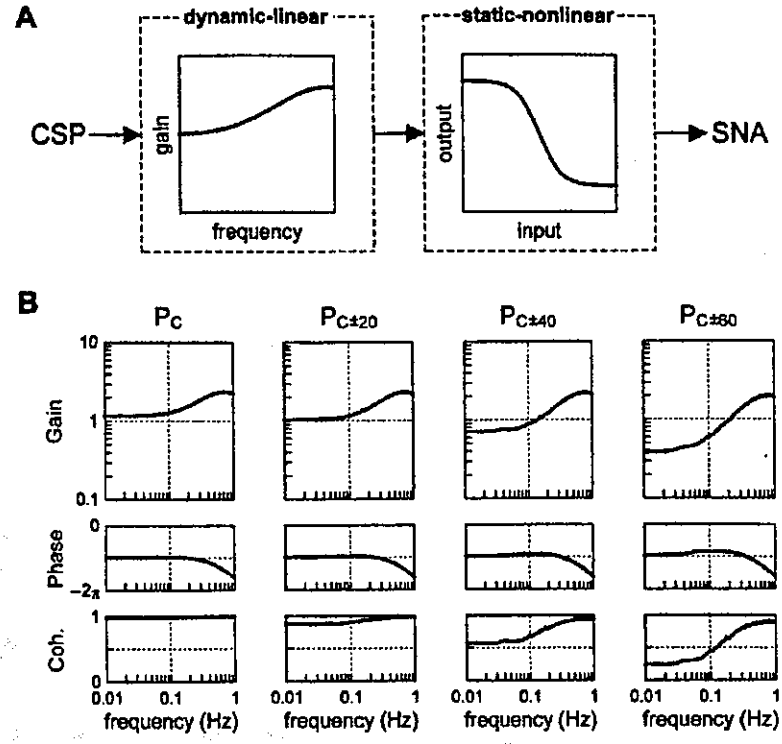

Fig. 1. *A*: a cascade model for the baroreflex neural arc comprised of a linear derivative filter followed by a nonlinear sigmoidal component (see appendix for details). CSP, carotid sinus pressure; SNA, sympathetic nerve activity. *B*: simulation results of the transfer function from CSP to SNA obtained by a binary white noise input. Mean input pressure was set at the center (P_C) of the sigmoidal nonlinearity and deviated by ±20, ±40, and ± 60 mmHg from P_C ($P_{C\pm20}$, $PC_{\pm40}$, and $PC_{\pm60}$, respectively). Coh, coherence.

(see appendix for numerical descriptions). This model was able to reproduce the input size dependence of baroreflex neural arc transfer characteristics from carotid sinus pressure (CSP) to SNA in a previous study (14). We calculated the linear transfer function of this model in the frequency range between 0.01 and 1 Hz by using a binary white noise input. The mean input pressure was deviated from the center (P_C) of the sigmoidal nonlinearity by ±20, ±40, and ±60 mmHg ($P_{C\pm20}$, $P_{C\pm40}$, and $P_{C\pm60}$, respectively).

Surgical preparations. Animals were cared for strictly in accordance with the *Guiding Principles for the Care and Use of Animals in the Field of Physiological Sciences* approved by the Physiological Society of Japan. Eight Japanese white rabbits weighing 2.6–3.6 kg were anesthetized by intravenous injection (2 ml/kg) of a mixture of urethane (250 mg/ml) and α-chloralose (40 mg/ml) and mechanically ventilated with oxygen-enriched room air. Supplemental anesthetics were injected as necessary (0.5 ml/kg) to maintain an appropriate level of anesthesia. AP was measured with a high-fidelity pressure transducer (Millar Instruments, Houston, TX) inserted via the right femoral artery. We isolated bilateral carotid sinuses from the systemic circulation by ligating the internal and external carotid arteries and other small branches originating from the carotid sinus regions. The isolated carotid sinuses were filled with warmed physiological saline through catheters inserted via the common carotid arteries. CSP was controlled by a servo-controlled piston pump. Bilateral vagal and aortic depressor nerves were sectioned at the neck to minimize reflex effects from the cardiopulmonary region and aortic arch on the central processing of the baroreflex neural arc. We exposed the left cardiac sympathetic nerve through a midline thoracotomy and attached a pair of stainless steel wire electrodes (Bioflex wire AS633; Cooner Wire) to record SNA (13). The nerve bundle peripheral to the electrodes was sectioned to eliminate afferent signals from the heart. The nerve and electrodes were covered with curing silicone glue (Kwik-Sil; World Precision Instruments) for insulation and fixation. The preamplified nerve signal was band-pass filtered at 150–1,000 Hz, and then full-wave rectified and low-pass filtered with a cutoff frequency of 30 Hz to quantify nerve activity. Pancuronium bromide (0.1 mg/kg) was administered to prevent contamination of muscular activity in the SNA recording. Body temperature was maintained at ~38°C with a heating pad.

Protocols. To estimate dynamic characteristics of the carotid sinus baroreflex at different operating points, we perturbed CSP with the mean input pressure set at 70, 100, 130, and 160 mmHg. These protocols are hereafter denoted as P_{70}, P_{100}, P_{130}, and P_{160}, respectively. In each protocol, CSP was assigned at either 20 mmHg above or below the mean input pressure every 500 ms according to a binary white noise signal. The four protocols were performed in random order. After mean SNA and AP had reached a steady state in each protocol, CSP, SNA, and AP were recorded for 10 min. Data were sampled at 200 Hz with a 12-bit analog-to-digital converter and stored on the hard disk of a dedicated laboratory computer system.

Data analysis. The neural arc transfer function from CSP to SNA, the peripheral arc transfer function from SNA to AP, and the total loop transfer function from CSP to AP were estimated by the following procedure. The input-output data pairs were resampled at 10 Hz and segmented into eight sets of 50%-overlapping bins of 1,024 points each (6). For each segment, a linear trend was subtracted and a Hanning window was applied. A fast Fourier transform was performed to obtain the spectra of the data segments (3). The ensemble averages of input [$S_{XX}(f)$] and output [$S_{YY}(f)$] and cross-spectra between the input and output [$S_{YX}(f)$] were estimated over the eight segments. Finally, the transfer function [$H(f)$] from the input to the output was calculated as (18)

$$H(f) = \frac{S_{YX}(f)}{S_{XX}(f)} \quad (1)$$

To quantify the linear dependence between the input and output signals in the frequency domain, a magnitude-squared coherence function [Coh(f)] was calculated as (18)

$$\mathrm{Coh}(f) = \frac{|S_{YX}(f)|^2}{S_{XX}(f)S_{YY}(f)} \quad (2)$$

tapraid4/zh4-ahea/zh4-ahea/zh400604/zh43109d04g | moyerr | S=6 | 3/30/04 | 17:09 | MS: H0787-3 | Ini: 06e/sa\dlh | Input-dms

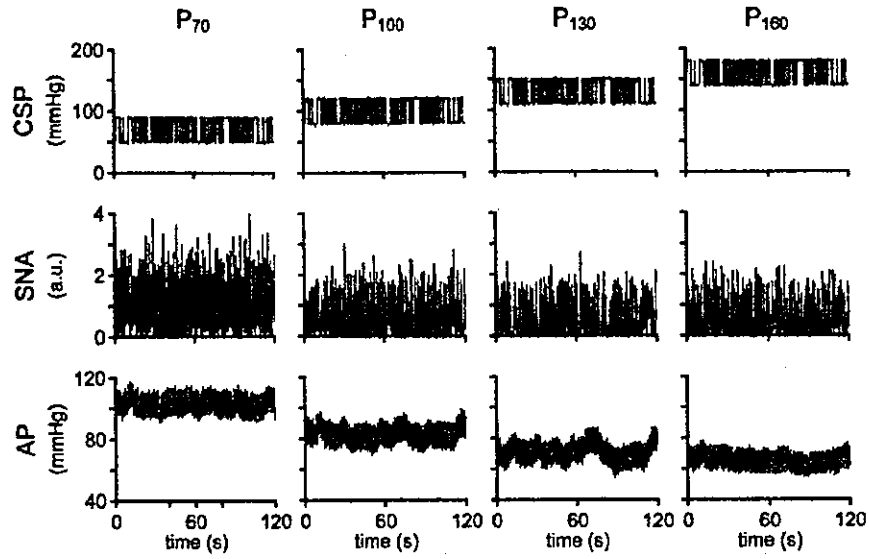

Fig. 2. Representative time series for CSP, SNA, and arterial pressure (AP) obtained from the 4 protocols. CSP was perturbed according to a binary white noise sequence. The mean levels of SNA and AP decreased as the mean input pressure increased. P_{70}, P_{100}, P_{130}, and P_{160}, protocols with mean input pressure at 70, 100, 130, and 160 mmHg, respectively; au, arbitrary units.

The coherence value ranges from zero to unity. A unity coherence value indicates perfect linear dependence between the input and output signals, whereas a zero coherence value indicates total independence between the two signals. Possible sources for lowering the coherence values include physical noise in signal measurements, biological noise in the output signal unrelated to the input signal, and nonlinear system responses.

Statistical analysis. All data are presented as means ± SD. Because the absolute amplitude of SNA varied depending on recording conditions, SNA is presented in arbitrary units (au). We calculated a normalization factor for the neural arc transfer function in each animal so that the average value of transfer gains obtained from the four protocols became unity at 0.01 Hz. Because we multiplied the same normalization factor to the transfer gain values at all frequencies, the gain plot did not change its frequency distribution. The inverse of the normalization factor was then applied to the peripheral arc transfer function in each animal. The total loop transfer function was not normalized. To compare the transfer functions among the P_{70}, P_{100}, P_{130}, and P_{160} protocols, the transfer gain values at 0.01 and 0.1 Hz ($G_{0.01}$ and $G_{0.1}$) were used. To quantify the extent of frequency-dependent changes in transfer gain, an average slope of the transfer gain between 0.1 and 0.5 Hz ($Slope_{0.1-0.5}$) was calculated. The frequencies of these parameters were chosen arbitrarily so that the parameters could properly represent the observed changes in the transfer functions. These parameters were tested among the four protocols with a repeated-measures analysis of variance followed by the Tukey test for all pairwise comparisons (5). Differences were considered significant when $P < 0.05$. Differences in mean SNA and AP during the CSP perturbation were tested among the four protocols by the same statistical procedure.

RESULTS

Figure 1*B* shows the linear transfer function from CSP to SNA estimated from the simulation data with a derivative-sigmoidal cascade model (see APPENDIX for details). Gain plots, phase plots, and coherence functions are presented. When the mean input pressure was at the center of the sigmoidal nonlinearity, the transfer gain increased slightly with increasing frequency. The phase approached $-\pi$ rad at the lowest frequency and lagged with increasing frequency. The coherence values were close to unity in the frequency range from 0.01 to AQ:4 1 Hz. The deviation of mean input pressure at $P_{C\pm20}$, $P_{C\pm40}$, and $P_{C\pm60}$ decreased the transfer gain mainly in the low-frequency range. The derivative characteristics became more enhanced as the deviation of mean input pressure increased. Although the phase plot did not change markedly across the four conditions, the phase values led slightly between 0.04 and 0.3 Hz at $P_{C\pm60}$. The deviation of mean input pressure decreased coherence values in the lower frequencies.

Figure 2 shows typical time series of CSP, SNA, and AP in F2 one animal. CSP was perturbed by a binary white noise sequence. An identical binary sequence with a different pressure level was imposed on CSP. Although the series are arranged in Fig. 2 in order of ascending CSP level, the actual protocols were performed in random order. The elevation of CSP level suppressed mean SNA and AP. Despite the same amplitude of CSP perturbation, changes in AP appeared to be greater in the P_{100} and P_{130} protocols than in the P_{70} and P_{160} protocols.

Mean levels of SNA and AP obtained from all animals are summarized in Table 1. The mean SNA and AP values during T1 the CSP perturbation were significantly higher in the P_{70} protocol than in the other three protocols. The mean AP value was significantly lower in the P_{160} protocol than in the P_{100} protocol.

Figure 3 shows the neural arc transfer functions averaged F3 from all animals. Gain plots, phase plots, and coherence functions are presented. The transfer gain increased with increasing frequency in each protocol, indicating the derivative characteristics of the neural arc. The gain values at lower

Table 1. *Mean levels of sympathetic nerve activity and arterial pressure*

	P_{70}	P_{100}	P_{130}	P_{160}
SNA, au	1.17±0.30*†‡	0.85±0.37	0.73±0.33	0.72±0.28
AP, mmHg	113±13*†‡	93±15	82±16	77±13§

Data are means ± SD. SNA, sympathetic nerve activity; au, arbitrary units; AP, arterial pressure; P_{70}, P_{100}, P_{130}, P_{160}, input pressure of 70, 100, 130, and 160 mmHg, respectively. *$P < 0.01$, †$P < 0.01$, ‡$P < 0.01$ vs. P_{100}, P_{130}, and P_{160}, respectively; §$P < 0.05$ vs. P_{100}.

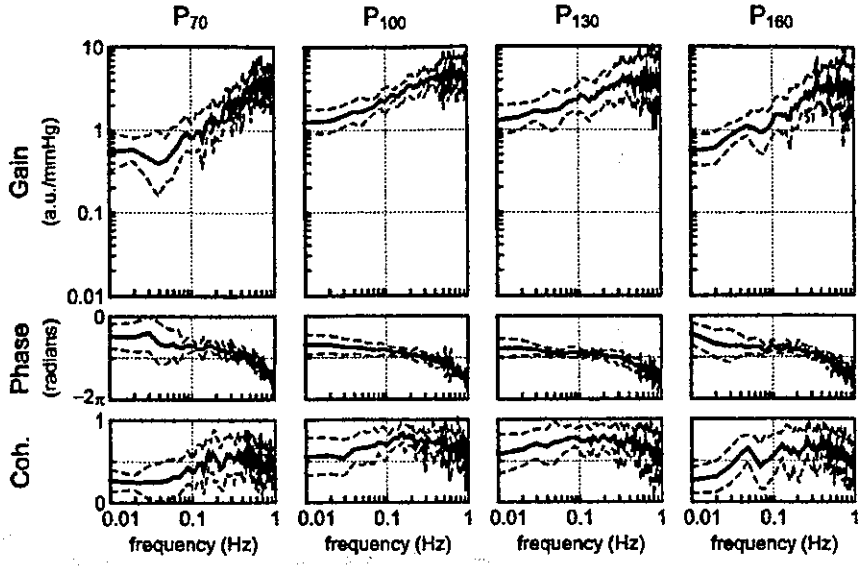

Fig. 3. Neural arc transfer functions obtained from the 4 protocols. The gain plots, phase plots, and coherence functions are shown. The transfer gain at 0.01 Hz was smaller in the P_{70} and P_{160} protocols than in the P_{100} and P_{130} protocols. The slope of increasing gain between 0.1 and 0.5 Hz was steeper in the P_{70} and P_{160} protocols than in the P_{100} and P_{130} protocols. Solid and dashed lines represent mean and mean ± SD values, respectively.

frequencies were smaller in the P_{70} and P_{160} protocols than in the P_{100} and P_{130} protocols. In contrast, the gain values above 0.5 Hz were similar among the four protocols. As a result, the slope of the increasing gain was steeper in the P_{70} and P_{160} protocols than in the P_{100} and P_{130} protocols The phase approached $-\pi$ rad at the lowest frequency in the P_{100} and P_{130} protocols, reflecting the out-of-phase relationship between CSP and SNA. The phase values in the lower frequencies were dispersed, and mean phase values were deviated from $-\pi$ toward 0 rad in the P_{70} and P_{160} protocols. The coherence values were <0.5 below 0.1 Hz in the P_{70} protocols. The coherence values appeared to be greater in the P_{100} and P_{130} protocols than in the P_{70} and P_{160} protocols.

F4 Figure 4 shows the peripheral arc transfer functions averaged from all animals. The transfer gain decreased with increasing frequency in each protocol, indicating the low-pass characteristics of the peripheral arc. The transfer gain values below 0.03 Hz were smaller in the P_{70} protocol than in the other three protocols. A sharp peak around 0.6 Hz corresponded to the frequency of artificial ventilation. The phase approached 0 rad at the lowest frequency in each protocol, reflecting the fact that an increase in SNA increased AP at steady state. The phase lagged significantly with increasing frequency in each protocol. The coherence values were <0.5 below 0.4 Hz in the P_{70} protocol. The coherence values appeared to be greater in the P_{100} and P_{130} protocols than in the P_{70} protocol. The coherence values were similar in the P_{100} and P_{160} protocols.

F5 Figure 5 depicts the total loop transfer function averaged from all animals. The transfer gain decreased as the frequency increased in each protocol, indicating the low-pass characteristics of the total baroreflex loop. The gain values below 0.1 Hz were smaller in the P_{70} and P_{160} protocols than in the P_{100} and P_{130} protocols. The phase approached $-\pi$ rad at lowest frequencies in the P_{100} and P_{130} protocols, reflecting the negative feedback attained by the total baroreflex loop. The phase

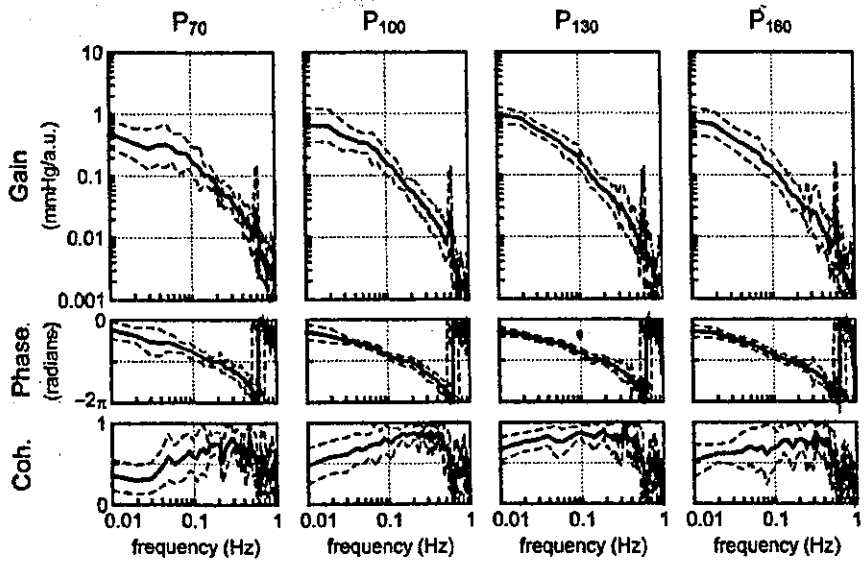

Fig. 4. Peripheral arc transfer functions obtained from the 4 protocols. The gain plots, phase plots, and coherence functions are shown. The transfer gain at 0.01 Hz was smaller in the P_{70} than in the P_{130} protocol. Neither the transfer gain at 0.1 Hz nor the slope of decreasing gain from 0.1 to 0.5 Hz differed among the 4 protocols. Solid and dashed lines represent mean and mean ± SD values, respectively.

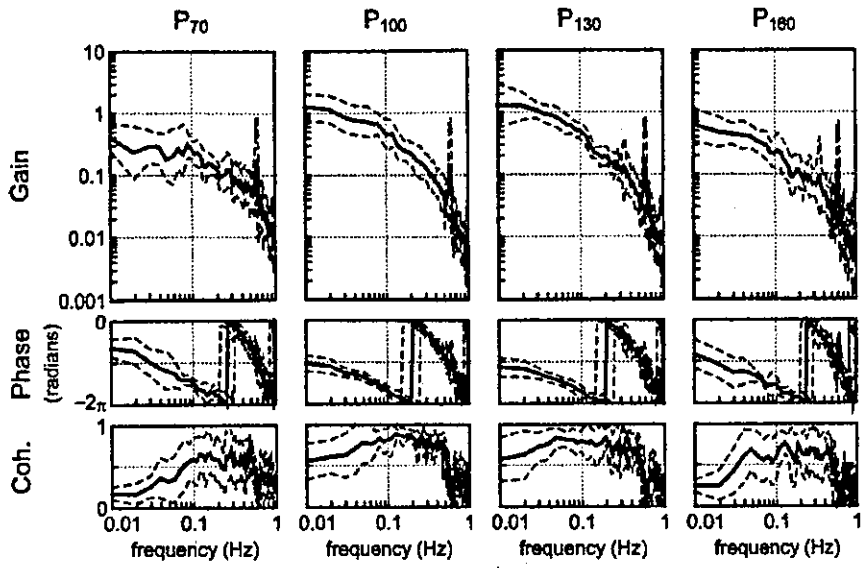

Fig. 5. Transfer functions of the total baroreflex loop obtained from the 4 protocols. The gain plots, phase plots, and coherence functions are shown. The transfer gain at 0.01 Hz was smaller in the P_{70} protocol than in the P_{100} and P_{130} protocols. The transfer gain at 0.1 Hz was smaller in the P_{70} and P_{160} protocols than in the P_{100} and P_{130} protocols. The slope of decreasing gain between 0.1 and 0.5 Hz was shallower in the P_{70} than in the P_{100} protocol. Solid and dashed lines represent mean and mean ± SD values, respectively.

values in the lower frequencies were dispersed and mean phase values were deviated from $-\pi$ toward 0 rad in the P_{70} and P_{160} protocols. The coherence values were <0.5 below 0.08 Hz in the P_{70} protocol and <0.5 below 0.02 Hz in the P_{160} protocol. The coherence values appeared to be greater in the P_{100} and P_{130} protocols than in the P_{70} and P_{160} protocols.

T2 Table 2 summarizes the statistical analysis of the obtained data. In the neural arc, $G_{0.01}$ and $G_{0.1}$ were significantly smaller in the P_{70} and P_{160} protocols than in the P_{100} and P_{130} protocols. $Slope_{0.1-0.5}$ was significantly steeper in the P_{70} and P_{160} protocols than in the P_{100} and P_{130} protocols. In the peripheral arc transfer function, $G_{0.01}$ was significantly smaller in the P_{70} than in the P_{130} protocol. $G_{0.1}$ and $Slope_{0.1-0.5}$ did not differ among the four protocols. In the total loop transfer function, $G_{0.01}$ was significantly smaller in the P_{70} protocol than in the P_{100} and P_{130} protocols. $G_{0.1}$ was significantly smaller in the P_{70} and P_{160} protocols than in the P_{100} and P_{130} protocols. $Slope_{0.1-0.5}$ was significantly less negative in the P_{70} than in the P_{100} protocol.

DISCUSSION

We have demonstrated that differences in mean input CSP significantly affect the linear transfer function of the baroreflex neural arc estimated by a binary white noise input (Fig. 3). Changes in the neural arc transfer function observed in the animal experiment were qualitatively consistent with predictions made by the derivative-sigmoidal cascade model (Fig. 1*B*), reinforcing the validity of this model as a first approximation of baroreflex neural arc transfer characteristics.

Operating point dependence of baroreflex transfer characteristics. In a previous study, we (14) postulated a simple model of the baroreflex neural arc consisting of a linear derivative filter followed by a nonlinear sigmoidal component based on the input size dependence of the neural arc transfer characteristics. The same model predicted that deviation of the mean input level from the center of sigmoidal nonlinearity would decrease the gain of signal transduction mainly in the low-frequency range (Fig. 1*B*). The midpoint pressure for the static input-output relationship between CSP and SNA was ~110–115 mmHg in anesthetized rabbits (12, 13). Hence, significant deviation of the mean input CSP from the midpoint pressure in the P_{70} and P_{160} protocols resulted in decreased transfer gain in the lower frequencies compared with the P_{100} and P_{130} protocols (Fig. 3). Generally, the interpretation of the estimated transfer function in the frequencies associated with low coherence values is difficult. This is because the low

Table 2. *Parameters of neural arc, peripheral arc, and total loop transfer functions*

	P_{70}	P_{100}	P_{130}	P_{160}
Neural arc				
$G_{0.01}$, au/mmHg	0.61±0.26†§	1.32±0.42	1.36±0.45	0.60±0.25†§
$G_{0.1}$, au/mmHg	0.86±0.31†§	2.34±0.77	2.46±0.96	1.30±0.59*‡
$Slope_{0.1-0.5}$, dB/decade	17.6±3.6†§	8.1±4.4	7.4±6.6	14.1±4.3†§
Peripheral arc				
$G_{0.01}$, mmHg/au	0.54±0.26‡	0.76±0.43	0.96±0.30	0.85±0.41
$G_{0.1}$, mmHg/au	0.22±0.11	0.19±0.08	0.22±0.09	0.16±0.10
$Slope_{0.1-0.5}$, dB/decade	−31.5±11.5	−35.6±5.2	−34.7±6.7	−33.4±7.9
Total baroreflex loop				
$G_{0.01}$	0.46±0.24*§	1.40±0.80	1.55±0.72	0.73±0.39
$G_{0.1}$	0.28±0.09*‡	0.53±0.22	0.52±0.14	0.24±0.12†§
$Slope_{0.1-0.5}$, dB/decade	−17.3±7.3*	−28.3±5.5	−26.0±11.2	−21.8±7.7

Data are means ± SD. $G_{0.01}$, $G_{0.1}$, transfer gain at 0.01 Hz and 0.1 Hz, respectively; $Slope_{0.1-0.5}$, average slope of transfer gain between 0.1 and 0.5 Hz. *$P < 0.05$, †$P < 0.01$ vs. P_{100}; ‡$P < 0.05$, §$P < 0.01$ vs. P_{130}.